Applications of Mathematics

Pavel Šolín; Karel Segeth

Non-uniqueness of almost unidirectional inviscid compressible flow

Applications of Mathematics, Vol. 49 (2004), No. 3, 247–268

Persistent URL: http://dml.cz/dmlcz/134568

49 (2004) APPLICATIONS OF MATHEMATICS No. 3, 247–268

NON-UNIQUENESS OF ALMOST UNIDIRECTIONAL INVISCID COMPRESSIBLE FLOW*

PAVEL ŠOLÍN, Houston, KAREL SEGETH, Praha

(Received March 25, 2002)

Abstract. Our aim is to find roots of the non-unique behavior of gases which can be observed in certain axisymmetric nozzle geometries under special flow regimes. For this purpose, we use several versions of the compressible Euler equations. We show that the main reason for the non-uniqueness is hidden in the energy decomposition into its internal and kinetic parts, and their complementary behavior. It turns out that, at least for inviscid compressible flows, a bifurcation can occur only at flow regimes with the Mach number equal to one (sonic states). Analytical quasi-one-dimensional results are supplemented by quasi-one-dimensional and axisymmetric three-dimensional finite volume computations. Good agreement between quasi-one-dimensional and axisymmetric results, including the presence of multiple stationary solutions, is presented for axisymmetric nozzles with reasonably small slopes of the radius.

Keywords: non-uniqueness, inviscid gas flow, compressible Euler equations, quasi-one-dimensional, axisymmetric, finite volume method

MSC 2000: 35L65, 65H10, 76H05, 76M25, 76N10, 76N15

1. INTRODUCTION

The theory of almost unidirectional inviscid flow of perfect gases in tubes, ducts, pipes and nozzles is a relatively well-explored discipline (see, e.g., [3], [4], [5], [6], [7], [9], [12], [14], [15]), which deserves a permanent industrial attention. Nevertheless, only surprisingly few remarks can be found in the literature on the non-unique behavior that these flows can exhibit at sonic and transonic regimes in nontrivial

* This work was partly supported by the Grants GP 102/01/D114 and 201/04/1305 of the Grant Agency of the Czech Republic.

axisymmetric geometries. It is our aim to provide some analytical and numerical insight into this phenomenon in the present paper.

In Paragraph 2.1 we briefly recall the derivation of a basic quasi-one-dimensional model for inviscid compressible flow from the stationary quasi-one-dimensional compressible Euler equations. Attention is given to a sufficiently precise mathematical formulation. Although the model is a classical one (see, e.g., [3], [4], [5], [6], [12], [14], most analytical results are limited to *simple* and *Laval* nozzles (probably due to their predominant industrial importance), where the non-uniqueness of solution does not appear. We investigate existence of non-unique solutions in Paragraph 2.2, and present a recursive algorithm for the construction of all exact solutions in general multiple nozzles in Paragraph 2.6, using some preliminary results obtained in Paragraphs 2.3, 2.4 and 2.5.

Section 4 uses a few flow examples to compare analytical results constructed by means of the recursive algorithm from Section 2 with corresponding numerical results, computed using a quasi-one-dimensional and an axisymmetric three-dimensional finite volume schemes described in Section 3.

2. Quasi-one-dimensional model

In this section we will analyze a quite simple basic model of almost unidirectional inviscid compressible flow, which at the same time offers a sufficiently complex description of the flow and is sufficiently transparent to have an analytical solution. Obviously, for real-life industrial simulations, advanced quasi-one-dimensional models (such as, e.g., the Fanno model discussed in [4], [5], [7], [9] including wall drag and turbulence effects, or a viscous model [11]) are recommended.

2.1. Derivation of the model

Let us consider a bounded interval $I = [x_a, x_b] \subset \mathbb{R}$, real constants $0 < R_{\min} \leqslant R_{\max}$ and a bounded real function $r(x)\colon\ I \to [R_{\min}, R_{\max}]$ describing the radius of an axisymmetric pipe or nozzle. For simplicity, we assume that $r(x)$ is once continuously differentiable in (x_a, x_b) and continuous in I, but the results presented in this paper are valid also for $r(x)$ continuous and only piecewise smooth. We define a varying cross-section $a(x) = \pi r^2(x)$ for $x \in I$.

Stationary quasi-one-dimensional compressible Euler equations. The stationary quasi-one-dimensional compressible Euler equations (with the varying cross-

section a) are considered in the usual form

$$\frac{\partial a(x)\varrho(x)u(x)}{\partial x} = 0, \tag{1}$$

$$\frac{\partial a(x)[\varrho(x)u^2(x) + p(x)]}{\partial x} = p(x)\frac{\partial a(x)}{\partial x}, \tag{2}$$

$$\frac{\partial a(x)u(x)[e(x) + p(x)]}{\partial x} = 0, \tag{3}$$

$x \in (x_a, x_b)$, which can be found, e.g., in [3], [4], [5], [6], [9], [12]. Here $\varrho(x)$, $u(x)$, $p(x)$, $e(x)$ mean the density, velocity, pressure and total energy density, respectively. Total energy density e is defined as a sum of its internal and kinetic parts by the relation $e = p/(\kappa - 1) + \varrho u^2/2$, where $\kappa \in (1, 3)$ is a real constant. The flow is assumed to obey the perfect gas state equation

$$p(x) = \varrho(x)R\theta(x) \tag{4}$$

where R is the gas constant and $\theta(x)$ the absolute temperature.

Transformation of the governing equations. It is well known that, due to the hyperbolicity of the compressible Euler equations, only piecewise smooth but generally discontinuous solutions can be expected. In our case, all *discontinuities* are *shocks* (simultaneous discontinuities in all of ϱ, u and p), as contact discontinuities are not relevant (see, e.g., [15]).

Along smooth parts of the solution, (1) and (3) are equivalent to

$$a(x)\varrho(x)u(x) = m, \tag{5}$$

$$\frac{\kappa p(x)}{(\kappa - 1)\varrho(x)} + \frac{1}{2}u^2(x) = h, \tag{6}$$

where the symbols m, h are real constants denoting the mass flux and enthalpy, respectively. The Rankine-Hugoniot conditions imply that m, h are conserved also at shocks (see, e.g., [15]).

As the rate of momentum ϱu is not conserved in (2) due to a source term on the right-hand side, we usually consider the conservation of entropy

$$S(x) = c_v \ln \frac{p(x)}{\varrho^\kappa(x)} + \text{const.} \tag{7}$$

on smooth parts of the solution (see, e.g., [3], [12]). Detailed derivation of (7) and further properties of the entropy S can be found, e.g., in [1], [3], [4], [5], [6], [9], 15]. At shocks, the Rankine-Hugoniot condition

$$p(x_+) = p(x_-)\frac{2\kappa M(x_-)^2 - \kappa + 1}{\kappa + 1} \tag{8}$$

(see, e.g., [3], [12], [15]) can be used instead of (7). Here $x \in I$ and $p(x_+)$, $p(x_-)$, $M(x_-)$ mean the downstream pressure limit and the upstream pressure and the Mach number (defined below) limits at the shock, respectively.

Therefore (2) can be replaced by the conservation of the quantity

$$\frac{p(x)}{\varrho^\kappa(x)} = s \tag{9}$$

along continuous parts of the solution. Finally, let us recall the speed of sound $c(x)$ and the Mach number $M(x)$, defined by

$$c(x) = (\kappa p(x)/\varrho(x))^{1/2}, \quad M(x) = |u(x)|/c, \tag{10}$$

respectively. The flow is called *subsonic* where $M(x) < 1$, *sonic* where $M(x) = 1$ and *isentropic* where the quantity s from (9) is conserved.

Let us briefly recall some basic achievements of the fluid mechanics in the following Lemma 2.1.

Lemma 2.1. *Shocks cannot occur in subsonic or sonic flow regions. A flow leaves a shock always at subsonic regime. The entropy S and the quantity s defined in (9) are discontinuous at shocks and always increasing with respect to the flow direction. Both of these quantities stay conserved except for shocks.*

Proof. See basic literature on fluid mechanics, e.g. [1]. □

Problem 1. Let I, r, a be as described in Paragraph 2.1. Consider boundary data $\varrho_a > 0$, $u_a > 0$, $p_a > 0$, $p_b > 0$. Let us put $m = a(x_a)\varrho_a u_a$, $h = \kappa p_a/((\kappa - 1)\varrho_a) + u_a^2/2$ according to (5) and (6), respectively. For a finite set $\mathcal{D} \subset (x_a, x_b)$ (corresponding to shocks), partitioning (x_a, x_b) into a finite number of non-overlapping open intervals $I_1, I_2, \ldots, I_d$ (ordered from the left to the right), we consider a sequence of constants $p_a/\varrho_a^\kappa = s_1 < s_2 < \ldots < s_d$. The set $\mathcal{D}$ and real functions ϱ, u, p defined in $I \setminus \mathcal{D}$ are sought such that

1. ϱ, u, p are bounded, positive and smooth in $I \setminus \mathcal{D}$;
2. ϱ, u, p satisfy (5), (6) in $I \setminus \mathcal{D}$ with the constants m, h, respectively;
3. ϱ, p satisfy (9) in $I \setminus \mathcal{D}$ with $p/\varrho^\kappa = s_k$ in I_k, for all $1 \leqslant k \leqslant d$;
4. ϱ, u, p satisfy (8) at all $x \in \mathcal{D}$;
5. $\varrho(x_a) = \varrho_a$, $u(x_a) = u_a$, $p(x_a) = p_a$, $p(x_b) = p_b$.

In what follows, we will solve Problem 1 instead of the original differential equations (1), (2), (3).

2.2. A model problem with a non-unique solution

Lemma 2.2. *If Problem* 1 *has a solution* ϱ, u, p, *there is a unique pair of values* $\varrho_b, u_b > 0$ *such that* $\varrho(x_b) = \varrho_b$, $u(x_b) = u_b$. *If* $p_b = p_a$, *then* $\varrho_b = \varrho_a$, $u_b = u_a$.

Proof. Let us assume that a solution to Problem 1 exists. Equations (5), (6), expressing the conservation of m, h in $I \setminus \mathcal{D}$, yield a quadratic equation for $u(x_b) = u_b$. It is easy to see that this equation has always one positive and one negative root. The negative one is eliminated in view of (5). Relation (5) yields also the density ϱ_b. The rest is easy to see. □

Theorem 2.1. *Let the radius* r *be as described in Paragraph* 2.1 *and moreover satisfy* $r(x_a) = r(x_b) = r_0 > 0$, $r(x) > r_0$ *for all* $x \in (x_a, x_b)$. *Let the boundary data of Problem* 1 *satisfy* $M_a = u_a/(\kappa p_a/\varrho_a)^{1/2} = 1$, $p_b = p_a$. *Then Problem* 1 *has exactly two solutions in* I, *both of them smooth in* (x_a, x_b).

Proof. According to Lemma 2.2, a solution of Problem 1 must satisfy $\varrho(x_b) = \varrho_a$. As $p_a/\varrho_a^\kappa = p(x_b)/\varrho^\kappa(x_b)$, Lemma 2.1 yields that $\mathcal{D} = \emptyset$. Thus, the relation (8) is not relevant. Putting (5) and (9) into (6), we obtain

$$\frac{\kappa s}{\kappa - 1}\varrho^{\kappa-1}(x) + \frac{m^2}{2a^2(x)\varrho^2(x)} - h = 0 \tag{11}$$

for all $x \in I$. For an $x \in I$, the equation (11) can be written in the form

$$f_\varrho(\varrho(x)) = 0, \tag{12}$$

with the implicit function

$$f_\varrho(\xi) = \frac{\kappa s}{\kappa - 1}\xi^{\kappa-1} + \frac{m^2}{2a^2(x)\xi^2} - h \tag{13}$$

defined for all $\xi \in (0, \infty)$. The function f_ϱ is smooth and it achieves its only minimum at

$$\xi_{\min} = \Big(\frac{m^2}{\kappa a^2(x) s}\Big)^{\frac{1}{\kappa+1}}. \tag{14}$$

The derivative f'_ϱ is negative in $(0, \xi_{\min})$ and positive in $(\xi_{\min}, \infty)$. Further, $f_\varrho(\xi_{\min}) = 0$ both for x_a and x_b. For all $x \in I$, the value of $f_\varrho(\xi_{\min})$ is a decreasing function of the cross-section $a(x)$. Thus, the equation (12) has exactly one positive root $\varrho_1(x) = \varrho_2(x) = \varrho_a$ for $x = x_a$, exactly two positive roots $0 < \varrho_1(x) < \varrho_2(x)$ for all $x \in (x_a, x_b)$ and exactly one positive root $\varrho_1(x) = \varrho_2(x) = \varrho_a$ for $x = x_b$. The implicit function theorem immediately yields that the functions $\varrho_1(x)$, $\varrho_2(x)$ are smooth in (x_a, x_b). Putting the solutions $\varrho_1(x)$, $\varrho_2(x)$ into the equation (5), we obtain two different positive smooth solutions $u_1(x)$, $u_2(x)$ for the velocity. Finally, using (9), we obtain the corresponding solutions $p_1(x)$, $p_2(x)$ for the pressure. □

Let us remark that in case of two positive roots $0 < \varrho_1(x) < \varrho_2(x)$ the Mach number $M_1(x)$ corresponding to the solution $\varrho_1(x)$, $u_1(x)$, $p_1(x)$ is greater than one, i.e. the corresponding flow state is supersonic. Analogously, the Mach number $M_2(x)$ corresponding to the solution $\varrho_2(x)$, $u_2(x)$, $p_2(x)$ is less than one and thus the corresponding flow state is subsonic.

2.3. Properties of sonic points

As we have seen in the previous paragraph, *sonic points* (points $x \in I$ such that $M(x) = 1$) play an important role in the existence of non-unique solutions to Problem 1. It is our aim to mention some of their further useful properties in this paragraph.

Lemma 2.3. *Let $\mathcal{D}, \varrho, u, p$ solve Problem* 1. *Let $x \in I \setminus \mathcal{D}$ be such that $M(x) = 1$. Then the solution of Problem* 1 *at x has the unique form*

$$
\begin{aligned}
u(x) &= \Big(\frac{2h(\kappa-1)}{\kappa+1}\Big)^{1/2}, \\
\varrho(x) &= \frac{m}{a(x)u(x)}, \\
p(x) &= \frac{(\kappa-1)\varrho(x)[h - u^2(x)/2]}{\kappa}.
\end{aligned} \tag{15}
$$

Proof. Immediate from (5), (6) using (10). □

Lemma 2.4. *Let $\mathcal{D}$, ϱ, u, p solve Problem* 1. *Let $x_1, x_2 \in I \setminus \mathcal{D}$, $x_1 < x_2$, $M(x_1) = M(x_2) = 1$ and $a(x_1) = a(x_2)$. Then ϱ, u, p are continuous in $[x_1, x_2]$.*

Proof. Using Lemma 2.3 with $a(x_1) = a(x_2)$, we obtain $\varrho(x_1) = \varrho(x_2)$, $p(x_1) = p(x_2)$. Thus, $p(x_1)/\varrho^\kappa(x_1) = p(x_2)/\varrho^\kappa(x_2)$. Lemma 2.1 implies the continuity of ϱ, u, p in $[x_1, x_2]$. This obviously means that there is no $\tilde{x} \in \mathcal{D}$, $x_1 < \tilde{x} < x_2$. □

Lemma 2.5. *Let $\mathcal{D}, \varrho, u, p$ solve Problem* 1. *Let $x_1, x_2 \in I \setminus \mathcal{D}$, $x_1 < x_2$, $M(x_1) = M(x_2) = 1$ and $a(x_1) \neq a(x_2)$. Then none of ϱ, u, p can be continuous in $[x_1, x_2]$. Moreover, necessarily it is $a(x_1) < a(x_2)$.*

Proof. Lemma 2.3 with $a(x_1) \neq a(x_2)$ yields that $\varrho(x_1) \neq \varrho(x_2)$, $p(x_1) \neq p(x_2)$. This and the conservation of m, h in $I \setminus \mathcal{D}$ yield that $p(x_1)/\varrho^\kappa(x_1) \neq p(x_2)/\varrho^\kappa(x_2)$. Lemma 2.1 implies that $p(x_1)/\varrho^\kappa(x_1) < p(x_2)/\varrho^\kappa(x_2)$. Relation (15) yields that this is only possible if $a(x_1) < a(x_2)$. □

Lemma 2.6. *Let $\mathcal{D}$, ϱ, u, p solve Problem 1. Let $x_1, x_2 \in I \setminus \mathcal{D}$, $x_1 < x_2$, and let ϱ, u, p be continuous in $[x_1, x_2]$.*

a) *If $M(x_1) < 1$ and $r(x)$ is decreasing in $[x_1, x_2]$ then $M(x)$ is increasing in $[x_1, x_2]$, but the relation $M(x) < 1$ is preserved in $[x_1, x_2)$.*

b) *If $M(x_1) < 1$ and $r(x)$ is increasing in $[x_1, x_2]$ then $M(x)$ is decreasing in $[x_1, x_2]$, and obviously $M(x) < 1$ in $[x_1, x_2]$.*

c) *If $M(x_1) > 1$ and $r(x)$ is decreasing in $[x_1, x_2]$ then $M(x)$ is decreasing in $[x_1, x_2]$, but the relation $M(x) > 1$ is preserved in $[x_1, x_2)$.*

d) *If $M(x_1) > 1$ and $r(x)$ is increasing in $[x_1, x_2]$ then $M(x)$ is increasing in $[x_1, x_2]$, and obviously $M(x) > 1$ in $[x_1, x_2]$.*

Proof. We put $s_1 = p(x_1)/\varrho^\kappa(x_1)$. Let $x \in (x_1, x_2)$. For ϱ, u, p continuous, the relations (5), (6) and (9) with (10) yield

$$u^2(x) = \frac{2(\kappa-1)h}{2/M^2(x) + \kappa - 1}, \tag{16}$$

$$\varrho(x) = \frac{m}{a(x)u(x)}, \tag{17}$$

$$s_1 = \frac{a^{\kappa-1}(x)(2(\kappa-1)h)^{(\kappa+1)/2}}{\kappa m^{\kappa-1} M^2(x)[2/M^2(x) + \kappa - 1]^{(\kappa+1)/2}}. \tag{18}$$

Relation (18) can be written as

$$M^2(x)(2/M^2(x) + \kappa - 1)^{(\kappa+1)/2} \frac{1}{a^{\kappa-1}(x)} = \frac{(2(\kappa-1)h)^{(\kappa+1)/2}}{\kappa m^{\kappa-1} s_1} = \text{const.} \tag{19}$$

We consider (19) as an implicit function for the Mach number M. An analysis of the shape of its solution (taking into account the monotonicity of r supposed in a) to d)) yields the monotone behavior of M. This analysis also yields that in a) and c), the existence of an $x \in (x_1, x_2)$ such that $M(x) = 1$ is contradictory to (19). □

Corollary 2.1. *Without loss of generality, we can assume that $M(x_a) \neq 1$ if the radius r does not have a local minimum at x_a (namely, using the implicit function f_ϱ from the proof of Theorem 2.1, it can be shown that there would be no solution to Problem 1). Thus, Lemma 2.6 excludes all possibilities for the existence of sonic points except for such $x \in I$ where the radius r achieves a local minimum.*

Corollary 2.1 together with Lemma 2.3 will play an important role in the construction of multiple solutions as we will be able to evaluate solution of Problem 1 at these points in the pipe or nozzle a priori. Now let us turn our attention to the solution of Problem 1. For the sake of simplicity, we will deal with two simplified situations

in Paragraphs 2.4 and 2.5 first. A general recursive algorithm will be designed in Paragraph 2.6.

2.4. Isentropic solutions to Problem 1

In this paragraph we will discuss existence of isentropic solutions to Problem 1 (i.e. solutions satisfying $\mathcal{D} = \emptyset$) and construct all of them if relevant.

Lemma 2.2 allows us to compute values $\varrho_b, u_b > 0$ such that the boundary conditions $\varrho(x_b) = \varrho_b$, $u(x_b) = u_b$ are satisfied by all solutions to Problem 1. We put

$$s = \frac{p_a}{\varrho_a^\kappa}, \quad s_b = \frac{p_b}{\varrho_b^\kappa}. \tag{20}$$

An isentropic solution to Problem 1 can exist only if $s = s_b$. In this case we proceed analogously as in the proof of Theorem 2.1. Equation (8) is not relevant and (5), (6), (9) yield (11). There is an isentropic solution to Problem 1 if (12) has at least one real root for all $x \in I$, i.e. if

$$f_\varrho(\xi_{\min}) \leqslant 0 \tag{21}$$

for all $x \in I$. It is easy to see that the value of $f_\varrho(\xi_{\min})$ is a decreasing function of the radius r. Therefore it is sufficient to verify the condition (21) only at the global minimum of r in I. All isentropic solutions to Problem 1 are constructed using all real roots of (12) in the whole interval I as described in the algorithm below. It is not difficult to see that nonunique continuous solutions appear only in the situation described in Theorem 2.1.

Algorithm for the construction of all isentropic solutions.

- Verify the necessary condition $s(x_1) = s(x_2)$ for the existence of an isentropic solution.
- Verify the sufficient and necessary condition (21) for the existence of an isentropic solution at the point y_{i_0} where the global minimum of r in $[x_1, x_2]$ is achieved.
- If an isentropic solution exists, cover the interval $[x_1, x_2]$ with a sufficiently fine equidistant partition $x_1 = y_1 < y_2 < \ldots < y_{N_0} = x_2$.
- For $i := 1, 2, \ldots, N_0 - 1$ do
  - Compute all real roots of the equation (12) at y_i. If there is exactly one real root, it has the meaning of a sonic density at y_i. If there are two real roots, they have the meaning of the subsonic and the supersonic (in the sense of the remark at the end of Paragraph 2.2) density at the point y_i.
  - For all real roots at y_i obtained in the previous step compute the pressure $p(y_i)$ and the velocity $u(y_i)$ to get a complete flow state (states) at y_i.

With a sufficiently fine partition of the interval $[x_1, x_2]$, the algorithm finds all isentropic solutions connecting the states at x_1 and x_2.

2.5. Solutions to Problem 1 with exactly one shock

Now let us discuss the existence of solutions to Problem 1 which contain exactly one shock ($\mathrm{card}(\mathcal{D}) = 1$) and construct all of them if relevant.

Analogously as in the previous case, Lemma 2.2 allows us to compute values $\varrho_b, u_b > 0$ such that the boundary conditions $\varrho(x_b) = \varrho_b$, $u(x_b) = u_b$ are satisfied by all solutions to Problem 1. We put

$$s = \frac{p_a}{\varrho_a^\kappa}, \quad s_b = \frac{p_b}{\varrho_b^\kappa}. \tag{22}$$

Problem 1 can have a solution containing exactly one shock only if $s < s_b$. Suppose that the one shock case occurs and let $\tilde{x} \in (x_a, x_b)$ be the position of the discontinuity. We put $\varrho_L = \varrho(\tilde{x}_-)$, $u_L = u(\tilde{x}_-)$, $p_L = p(\tilde{x}_-)$, $\varrho_R = \varrho(\tilde{x}_+)$, $u_R = u(\tilde{x}_+)$, $p_R = p(\tilde{x}_+)$. Solutions of Problem 1 with exactly one shock at $\tilde{x}$ must satisfy the following three conditions:

1. Equations (5), (6), (9) with the boundary data $\varrho(x_a) = \varrho_a$, $u(x_a) = u_a$, $p(x_a) = p_a$, $\varrho(\tilde{x}_-) = \varrho_L$, $u(\tilde{x}_-) = u_L$, $p(\tilde{x}_-) = p_L$ are satisfied in $[x_a, \tilde{x})$.
2. Equations (5), (6), (9) with the boundary data $\varrho(\tilde{x}_+) = \varrho_R$, $u(\tilde{x}_+) = u_R$, $p(\tilde{x}_+) = p_R$, $\varrho(x_b) = \varrho_b$, $u(x_b) = u_b$, $p(x_b) = p_b$ are satisfied in $(\tilde{x}, x_b]$.
3. Values $p(\tilde{x}_-)$, $p(\tilde{x}_+)$ and $M(x_+) = |u(x_+)|/(\kappa p(x_+)/\varrho(x_+))^{1/2}$ satisfy the Rankine-Hugoniot relation (8).

The reader may note that isentropic solutions in $[x_a, \tilde{x})$ and $(\tilde{x}, x_b]$, required in items 1 and 2, need not be unique if geometrical situation from Theorem 2.1 occurs. Conditions 1 to 3 can be translated into the following system of nonlinear algebraic equations

$$\frac{\kappa p_L}{(\kappa - 1)(p_L/s)^{1/\kappa}} + \frac{m^2}{2a^2(\tilde{x})(p_L/s)^{2/\kappa}} - h = 0, \tag{23}$$

$$\frac{\kappa p_R}{(\kappa - 1)(p_R/s_b)^{1/\kappa}} + \frac{m^2}{2a^2(\tilde{x})(p_R/s_b)^{2/\kappa}} - h = 0, \tag{24}$$

$$\mathcal{R}(p_L, p_R) = p_R - \frac{2m^2(s/p_L)^{1/\kappa}/a^2(\tilde{x}) - (\kappa - 1)p_L}{\kappa + 1} = 0 \tag{25}$$

for unknowns $\tilde{x}$, p_L, p_R. Here $\mathcal{R}$ is a residuum of the Rankine-Hugoniot relation (8). The equation (25) is solved iteratively, using a sufficiently fine equidistant partition of I for initial guesses of $\tilde{x}$ and nested iterative procedures for the solution of (23), (24).

Algorithm for the construction of solutions with exactly one shock

- Verify the necessary condition $s(x_1) < s(x_2)$ for existence of a solution with exactly one shock.
- If the previous verification was successful, cover the interval $[x_1, x_2]$ with a sufficiently fine equidistant partition $x_1 = y_1 < y_2 < \ldots < y_{N_1} = x_2$.
- For $i := 1, 2, \ldots, N_1 - 1$ do
  - Compute the supersonic roots (in the sense of the remark in the end of Paragraph 2.2) of the equation (23) at the points y_i, y_{i+1} and denote them by $\tilde{p}_{L_1}$, $\tilde{p}_{L_2}$, respectively.
  - Compute the subsonic roots of the equation (24) at y_i, y_{i+1} and denote them by $\tilde{p}_{R_1}$, $\tilde{p}_{R_2}$, respectively.
  - Compute the values $\mathcal{R}(\tilde{p}_{L_1}, \tilde{p}_{R_1})$, $\mathcal{R}(\tilde{p}_{L_2}, \tilde{p}_{R_2})$ from (25). If their signs differ, resolve the value of $\tilde{x} \in [y_i, y_{i+1}]$ by means of the interval bisection method with a sufficient accuracy. In our code we use 10^{-10}.
  - Compute the density and the velocity ϱ_L, u_L and ϱ_R, u_R at $\tilde{x}$ using the obtained values of p_L, p_R, respectively, and the values of m, h.
  - Verify that the state ϱ_1, u_1, p_1 at x_1 can be isentropically connected with the state ϱ_L, u_L, p_L at $\tilde{x}$ and find all possible connections as described in Paragraph 2.4.
  - Verify that the state ϱ_R, u_R, p_R at $\tilde{x}$ can be isentropically connected with the state ϱ_2, u_2, p_2 at x_2 and find all possible connections as described in Paragraph 2.4.

With a sufficiently fine partition of the interval $[x_1, x_2]$, the algorithm finds all single shock solutions connecting the states at x_1 and x_2.

2.6. Algorithm for the construction of all solutions to Problem 1

Finally, we can introduce a recursive algorithm for the construction of all solutions to Problem 1 in this paragraph.

Analogously as in Paragraphs 2.4 and 2.5, Lemma 2.2 allows us to compute values $\varrho_b, u_b > 0$ such that boundary conditions $\varrho(x_b) = \varrho_b$, $u(x_b) = u_b$ are satisfied by all solutions to Problem 1. We put

$$s = \frac{p_a}{\varrho_a^\kappa}, \quad s_b = \frac{p_b}{\varrho_b^\kappa}. \tag{26}$$

If $s > s_b$, there is no solution to Problem 1 due to Lemma 2.1. If $s = s_b$, there can be only isentropic solutions to Problem 1. We use the algorithm designed in Paragraph 2.4. If $s < s_b$, we can expect only discontinuous solutions. All solutions to Problem 1 containing exactly one shock are constructed as shown in Paragraph 2.5.

Before we start constructing solutions with multiple shocks, it is natural to ask how many of them can be expected.

Lemma 2.7. *Let $I_0 = [x_1, x_2] \subset I$ and r be constant in I_0. Let Problem 1 have a solution. If the solution is subsonic or sonic in I_0, it is necessarily constant in I_0. If $M(x_1) > 1$, the solution is either constant in I_0 or piecewise constant with exactly one shock in I_0. In the case of shock, the solution of Problem 1 is not unique because all shock positions $x_s \in I_0$ are possible.*

Proof. In the subsonic or sonic case, no shock occurs due to Lemma 2.1. Using (5), (6), (9) and $r = \text{const.}$ in I_0, we obtain that ϱ, u, p can be only constant in I_0. If $M(x_1) > 1$ and no shock occurs, the solution is constant for the same reason as before. If there is a shock (at most one due to Lemma 2.1) at an $x_s \in I_0$, (5), (6), (9) are conserved in both intervals $[x_1, x_s)$, $(x_s, x_2]$, obviously with different constants $0 < s_1 < s_2$ in (9), respectively. There is no preferred position for the shock with respect to solvability of Problem 1. □

Estimation of the maximal number of shocks. Let us consider all local minima of the radius r, except for the endpoints x_a, x_b (if relevant), and collect them into a set

$$\mathcal{P} = \{P_1, P_2, \dots, P_N\} \subset I. \tag{27}$$

If this minimum is not unique due to a constant radius section $I_0 \subset I$, we can identify the corresponding $x \in \mathcal{P}$ with I_0 in the sense of Lemma 2.7. According to Corollary 2.1, $M(x) = 1$ can occur only if $x \in \mathcal{P}$. Lemma 2.1 yields that the maximal number of shocks in the pipe or nozzle is $N_{\max} = N$ if the inlet is subsonic and $N_{\max} = N + 1$ if the inlet is supersonic.

Construction of solutions to Problem 1 with at least two shocks. We construct all solutions to Problem 1 with more than one shock using the following recursive algorithm:

- First we find all solutions to Problem 1 containing exactly two shocks, using all candidates for sonic points from $\mathcal{P}$: for all $i := 1, 2, \dots, N$ do
  - Put $M(P_i) = 1$.
  - Compute the solution $\varrho_i = \varrho(P_i)$, $u_i = u(P_i)$, $p_i = p(P_i)$ of Problem 1 at P_i using Lemma 2.3.
  - Consider Problem $1^{1,i}$ which is a subproblem of Problem 1 in the interval $I^{1,i} = [x_a, P_i]$, with boundary conditions $\varrho(x_a) = \varrho_a$, $u(x_a) = u_a$, $p(x_a) = p_a$, $p(P_i) = p_i$.
  - Consider Problem $1^{2,i}$ which is also a subproblem of Problem 1 in the interval $I^{2,i} = [P_i, x_b]$, with boundary conditions $\varrho(P_i) = \varrho_i$, $u(P_i) = u_i$, $p(P_i) = p_i$, $p(x_b) = p_b$.

- Find all solutions containing exactly one shock to both Problem $1^{1,i}$ and Problem $1^{2,i}$, using the algorithm designed in Paragraph 2.5.
- Construct all solutions to Problem 1 as all pairs $[\mathcal{S}^{1,i}, \mathcal{S}^{2,i}]$, where $\mathcal{S}^{1,i}$ solves Problem $1^{1,i}$ and $\mathcal{S}^{2,i}$ solves Problem $1^{2,i}$.

- Analogously find all solutions containing $k = 3, 4, \ldots, N_{\max}$ shocks: Put $M(P_j) = 1$ for all subsets of $\mathcal{P}$ containing exactly $k - 1$ elements. For each of these subsets, interval I is partitioned into k subintervals where k subproblems to Problem 1 are defined. To each of these subproblems, all solutions containing exactly one shock are constructed using the algorithm from Paragraph 2.5. Let us remark that some combinations of these subproblems can be excluded a priori in the sense of Lemmas 2.4 and 2.5. Finally, we merge the solutions of the subproblems analogously as in the previous case of exactly two shocks.

Let us remark that for quasi-one-dimensional geometries with several local minima of the radius r, there may be a considerable number of solutions due to the large number of combinations of the sonic points P_i. Discontinuous solutions contain stable as well as unstable shocks. It can be shown that the stable ones occur only in divergent parts of the pipe or nozzle while those positioned within convergent parts are unstable. Diagrams of the dependence of the number and positions of stable and unstable shocks on the boundary conditions turn out to have a very interesting structure. This work is currently under development.

3. Brief description of numerical schemes

Both the quasi-one-dimensional and axisymmetric three-dimensional compressible Euler equations are nonconservative, and therefore difficult to discretize by standard finite volume schemes. Thus, we briefly describe a quasi-one-dimensional scheme and develop a suitable version of the axisymmetric three-dimensional finite volume method in this section. Readers who are not familiar with the finite volume discretization of the compressible Euler equations are kindly asked to look into a book or a paper, e.g. [2], [8], [13].

Quasi-one-dimensional finite volume method. This version of the finite volume method is similar to the purely one-dimensional one. Nonconservativity of the quasi-one-dimensional compressible Euler equations can be overcome taking into account numerical flux through solid walls of the pipe or nozzle. This can be done in the same way as in three-dimensionsional finite volume schemes. Obviously, variable cross-section a is used instead of the unit one in the purely one-dimensional scheme.

Axisymmetric finite volume method. One possible way to derive an axisymmetric finite volume scheme is to start directly from the axisymmetric compressible Euler equations. However, source terms appearing on their right-hand side are a source

of considerable difficulties and numerical errors. Therefore we decided to propose another approach, which is not frequently mentioned in the literature and which significantly reduces nonconservativity problems. We start from the three-dimensional compressible Euler equations, discretize them by a three-dimensional finite volume scheme, and apply the axisymmetry of the problem to the discretized problem.

Let us consider a two-dimensional domain Ω defined by

$$\Omega = \{[x,y] \in \mathbb{R}^2;\ x \in (x_a, x_b),\ y \in (0, r(x))\} \tag{28}$$

and cover it with a standard unstructured finite element triangulation

$$\tau_h = \{T_1, T_2, \ldots, T_M\}. \tag{29}$$

By $K(i)$ we denote the set of indices of triangles $T_j \in \tau_h$, $j = 1,2,\ldots,M$, $j \neq i$, which have a common side with the triangle $T_i \in \tau_h$, $i = 1,2,\ldots,M$.

Let us consider an angle $\varphi \in [0, 2\pi)$ and the plane Σ constructed by the rotation of the (x,y) plane around its x-axis by the angle φ. This rotation defines a new Cartesian coordinate system $(\tilde{x}, \tilde{y}, \tilde{z})$, where $\tilde{x} \equiv x$ and the plane Σ is identical with the plane $(\tilde{x}, \tilde{y})$.

We consider a velocity vector $\boldsymbol{u} = (u_x, u_y, u_z)^T$ parallel to the plane Σ. In the new coordinate system, $\boldsymbol{u}$ can be expressed as $\tilde{\boldsymbol{u}} = (\tilde{u}_x, \tilde{u}_r, 0)^T$ with $u_y = \tilde{u}_r \cos\varphi$, $u_z = \tilde{u}_r \sin\varphi$. The rotation matrix $\overline{Q}$ transforming vectors from the new coordinate system to the original one has the form

$$\overline{Q} = \begin{pmatrix} 1 & 0 & 0 \\ 0 & \cos\varphi & -\sin\varphi \\ 0 & \sin\varphi & \cos\varphi \end{pmatrix}. \tag{30}$$

Obviously $\boldsymbol{u} = \overline{Q}\tilde{\boldsymbol{u}}$ and $\overline{Q}\overline{Q}^T = I$. Conservation state vectors $\boldsymbol{w} = (\varrho, \varrho u_x, \varrho u_y, \varrho u_z, e)^T$ (ϱ and e mean the fluid density and total energy density, respectively) such that the corresponding velocity vector $\boldsymbol{u} = (u_x, u_y, u_z)^T$ is parallel to Σ, can be expressed in the new coordinate system as $\tilde{\boldsymbol{w}} = (\varrho, \varrho\tilde{u}_x, \varrho\tilde{u}_r, 0, e)^T$. The transformation matrix $\mathcal{Q} \in \mathbb{R}^5 \times \mathbb{R}^5$ defined by

$$\mathcal{Q} = \begin{pmatrix} 1 & 0 & 0 \\ 0 & \overline{Q} & 0 \\ 0 & 0 & 1 \end{pmatrix}, \tag{31}$$

where 0 may denote also a zero row or column vector, transforms state vectors from the new coordinate system to the original one. Obviously, $\boldsymbol{w} = \mathcal{Q}\tilde{\boldsymbol{w}}$.

The angular flux $\boldsymbol{f}_\varphi$ has the form $\boldsymbol{f}_\varphi(\boldsymbol{w}) = -p(\boldsymbol{w})(0,0,\sin\varphi,-\cos\varphi,0)^T$ for conservation states $\boldsymbol{w}$ with velocity vectors parallel to the plane Σ. The function $p(\boldsymbol{w})$ expressing the pressure corresponding to a conservation state $\boldsymbol{w}$ has the form $p(\boldsymbol{w}) = (\kappa-1)(w_3-(w_2^2+w_3^2+w_4^2)/(2w_1))$. We will need the angular derivative of $\boldsymbol{f}_\varphi$, which has the form

$$\frac{\partial}{\partial\varphi}\boldsymbol{f}_\varphi(\boldsymbol{w}) = -p(\boldsymbol{w})(0,0,\cos\varphi,\sin\varphi,0)^T = -p(\boldsymbol{w})\mathcal{Q}(0,0,1,0,0)^T. \tag{32}$$

Now we can proceed to the finite volume method: Each triangle $T_i \in \tau_h$ represents a three-dimensional axisymmetric ring

$$R_i = \{[x,y,z] \in \mathbb{R}^3,\ x = \bar{x},\ y = \bar{y}\sin\psi,\ z = \bar{y}\cos\psi,\ [\bar{x},\bar{y}] \in T_i,\ 0 \leqslant \psi < 2\pi\}. \tag{33}$$

By $|R_i|$ we denote the volume of the ring R_i. We put $S_{ij} = \overline{R}_i \cap \overline{R}_j$, $1 \leqslant i \leqslant M$, $j \in K(i)$, $j \neq i$ and by $|S_{ij}|$ denote the surface size of S_{ij}. By $R_i(\Delta\varphi)$ we denote a segment of the ring R_i of a small angular width $\Delta\varphi > 0$, lying between the angles $\varphi - \Delta\varphi/2$, $\varphi + \Delta\varphi/2$. The corresponding section of the surface S_{ij} will be denoted by $S_{ij}(\Delta\varphi)$.

Let us consider two time-dependent conservation state vectors $\boldsymbol{w}_i(t), \boldsymbol{w}_j(t) \in \mathbb{R}^5$ corresponding to segments $R_i(\Delta\varphi)$, $R_j(\Delta\varphi)$, a normal vector ν_{ij} to $S_{ij}(\Delta\varphi)$ lying in Σ, and a standard three-dimensional numerical flux $H(\boldsymbol{w}_i(t), \boldsymbol{w}_j(t), \nu_{ij})$: $\mathbb{R}^5 \times \mathbb{R}^5 \times \mathbb{R}^3 \to \mathbb{R}^5$ (see, e.g., [2], [1] for its definition and properties). With $\boldsymbol{w}(t) = \mathcal{Q}\tilde{\boldsymbol{w}}(t)$, $\nu_{ij} = \overline{\mathcal{Q}}\tilde{\nu}_{ij}$ we can transform the numerical flux H into the new coordinates using its *rotational invariance* as follows,

$$H(\boldsymbol{w}_i(t), \boldsymbol{w}_j(t), \nu_{ij}) = H(\mathcal{Q}\tilde{\boldsymbol{w}}_i(t), \mathcal{Q}\tilde{\boldsymbol{w}}_j(t), \overline{\mathcal{Q}}\tilde{\nu}_{ij}) = \mathcal{Q}H(\tilde{\boldsymbol{w}}_i(t), \tilde{\boldsymbol{w}}_j(t), \tilde{\nu}_{ij}). \tag{34}$$

Semi-discretizing the three-dimensional compressible Euler equations in space over the segment $R_i(\Delta\varphi)$, we obtain

$$\begin{aligned}\frac{\Delta\varphi}{2\pi}|R_i|\dot{\boldsymbol{w}}_i(t) + \sum_{j\in K(i)} \frac{\Delta\varphi}{2\pi}|S_{ij}|H(\boldsymbol{w}_i(t), \boldsymbol{w}_j(t), \nu_{ij}) \\ + |T_i|(\boldsymbol{f}_{\varphi+\Delta\varphi/2}(\boldsymbol{w}_i(t)) - \boldsymbol{f}_{\varphi-\Delta\varphi/2}(\boldsymbol{w}_i(t))) = 0,\end{aligned} \tag{35}$$

where $|T_i|$ is the area of the triangle $T_i \in \tau_h$. The second term in (35) corresponds to surface sections $S_{ij}(\Delta\varphi)$ of the segment $R_i(\Delta\varphi)$, $j \in K(i)$, and the last term on the left-hand side to the angular fluxes through the segment $R_i(\Delta\varphi)$.

Expressing the state vectors $\boldsymbol{w}_i(t)$, $\boldsymbol{w}_j(t)$ in the new coordinate system, using the property $\mathcal{Q}\mathcal{Q}^T = I$, passing to the limit

$$\lim_{\Delta\varphi\to 0} \frac{\boldsymbol{f}_{\varphi+\Delta\varphi/2}(\boldsymbol{w}_i(t)) - \boldsymbol{f}_{\varphi-\Delta\varphi/2}(\boldsymbol{w}_i(t))}{\Delta\varphi} = \frac{\partial}{\partial\varphi}\boldsymbol{f}_\varphi(\boldsymbol{w}_i(t)) \tag{36}$$

and using (32), we finally obtain

$$\dot{\tilde{w}}_i(t) = -\frac{1}{|R_i|}\sum_{j\in K(i)} |S_{ij}| H(\tilde{w}_i(t), \tilde{w}_j(t), \tilde{\nu}_{ij}) + \frac{2\pi|T_i|}{|R_i|} p(\tilde{w}_i(t))(0,0,1,0,0)^T. \tag{37}$$

As the fourth component of all vectors in (37) is zero, (37) represents a two-dimensional finite volume method. Note that this axisymmetric scheme is similar to the standard two-dimensional one (see, e.g., [2], [1], [13]), using the ring volume $|R_i|$ and the common surface section size $|S_{ij}|$ where the triangle size $|T_i|$ and the common edge size $|\Gamma_{ij}|$ are used in the purely two-dimensional scheme, respectively. Moreover, an additional nonconservative pressure term

$$\frac{2\pi|T_i|}{|R_i|} p(\tilde{w}_i(t))(0,0,1,0,0)^T, \tag{38}$$

which is not necessary in the purely two-dimensional scheme, must be used in (37).

4. Numerical examples

In this section we will present a few examples of multiple solutions in simpler quasi-one-dimensional geometries. First let us give some background for the finite volume computations which will be performed using the quasi-1D and axisymmetric schemes described in Section 3.

In Paragraphs 2.4, 2.5 and 2.6 the reader saw that all exact solutions in the quasi-1D case can be computed in a straitforward way using a sufficiently fine division of the interval I. It is also not difficult to compute *some* of the multiple solutions numerically. In such case, one only needs to choose an arbitrary admissible initial condition and the finite volume scheme converges to one of the multiple solutions. However, the situation is much more complicated if we decide to compute *all* of the multiple solutions numerically.

The task to design the initial and boundary conditions for a compressible flow computation in such a way that the resulting stationary state matches a prescribed steady solution is an extremely difficult nonlinear inverse problem that (at least up to our best knowledge) has not yet been solved. Therefore we must satisfy ourselves with a simpler approach based on the solution of direct problems with the variation of the initial condition and application of time-dependent boundary conditions.

In our case, as the computational geometries are relatively simple, it will be sufficient to use time-independent boundary conditions matching those corresponding to

the exact solution. The choice of the initial conditions is more delicate. One possible way how to construct them is to make sure that they lie sufficiently close to the exact quasi-1D (time-independent) solution. Otherwise one can often observe that the finite volume method tends to switch over to a different candidate from the set of multiple solutions, typically to a solution with a lower energy.

For all quasi-1D as well as axisymmetric finite volume computations presented in this section, the initial condition was chosen as piecewise constant by averaging the exact quasi-1D solution in the axisymmetric sense over a suitably chosen coarse subdivision of the interval I. In case of the double nozzle (Paragraph 4.1) we used 20 equally long subelements. Thirty equally long subelements were used for the triple nozzle in Paragraph 2.4.

In both following paragraphs we will use the function

$$r(x) = \begin{cases} -\dfrac{\cos(10\pi(x-0.05))}{50} + 0.0265, & x \in [x_a, 0.05], \\ -\dfrac{\sin(10\pi x)}{250} + x/100 + 1/100, & x \in [0.05, x_b] \end{cases} \tag{39}$$

with $x_a < 0.05 < x_b$ for the definition of the radius of a nozzle.

4.1. A double nozzle

We have chosen this device as it is possible to find some discussions on its behavior in the literature (see, e.g., [3], [12]). Nevertheless, those discussions are mostly based on experimental experience. The device is called a *double nozzle* as the radius r has two local minima in the interval of interest (see Fig. 1). In this case we choose $I = [x_a, x_b]$ with $x_a = -0.05\,\mathrm{m}$, $x_b = 0.35\,\mathrm{m}$.

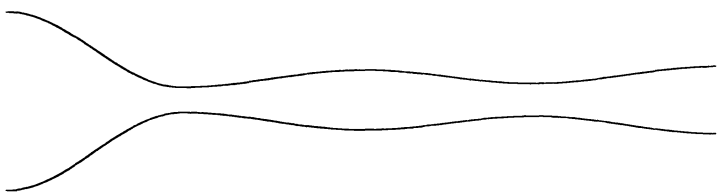

Figure 1. Geometry of the double nozzle.

We assume that the reservoir on the left-hand side is filled with almost quiet air of pressure $p_a = 50000\,\mathrm{Pa}$ and temperature $\theta_a = 368.16\,\mathrm{K}$. We choose a value $p_b = 15000$ Pa for the outer pressure. The positive inlet velocity u_a is computed in such a way that the nozzle works in the Laval regime. This regime describes free reservoir outflow with a maximal mass flux and is of crucial practical importance (see, e.g., [3], [12]. The density ϱ_a is computed from (4). In the Laval regime, the flow is sonic at such $x \in I$ where the radius r achieves its global minimum in I.

The interval I is covered with an equidistant partition of $N_{\text{elem}} = 1000$ finite volumes. In Figs. 2 and 3, two different analytical solutions to Problem 1 (obtained as described in Paragraph 2.6) are drawn by solid lines, while dashed lines represent always the corresponding steady solution of the quasi-one-dimensional finite volume scheme discussed in Section 3. In Figs. 4, 5, 6 and 7 we present steady results obtained with the axisymmetric scheme described in Section 3, corresponding to a structured triangular grid with 3000 elements.

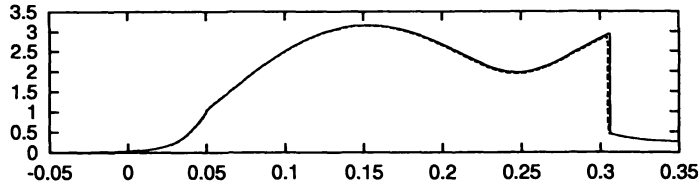

Figure 2. Mach number, quasi-one-dimensional exact (solid line) and steady finite volume (dashed line) solution with exactly one shock.

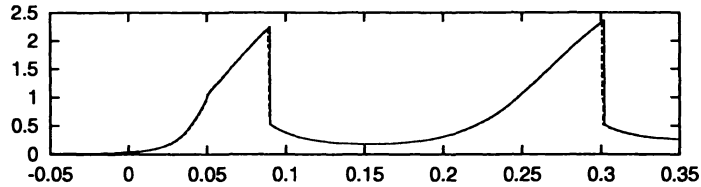

Figure 3. Mach number, quasi-one-dimensional exact (solid line) and steady finite volume (dashed line) solution with two shocks.

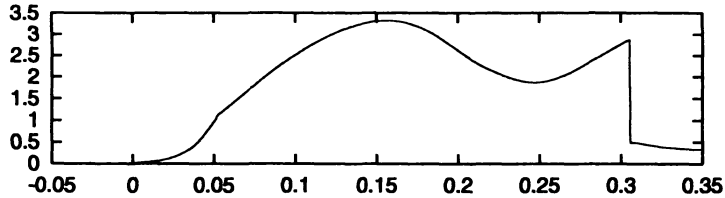

Figure 4. Mach number along the axis, steady three-dimensional axisymmetric finite volume solution with exactly one shock.

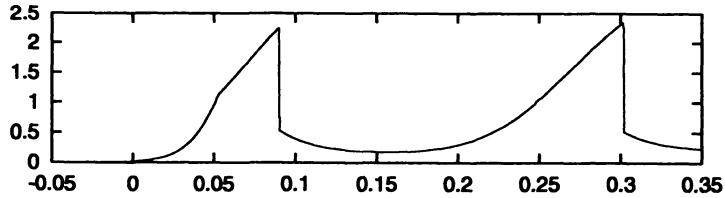

Figure 5. Mach number along the axis, steady three-dimensional axisymmetric finite volume solution with two shocks.

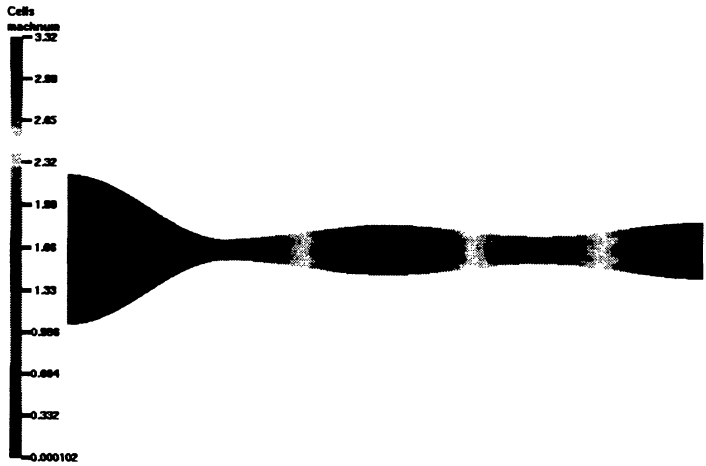

Figure 6. Mach number gray scale map, steady three-dimensional axisymmetric finite volume solution with exactly one shock.

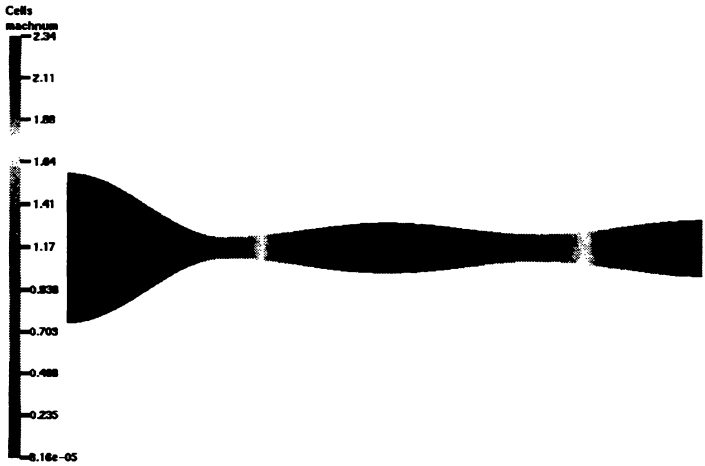

Figure 7. Mach number gray scale map, steady three-dimensional axisymmetric finite volume solution with two shocks.

4.2. A triple nozzle

Let us present an example of a *triple nozzle*, which is not frequently discussed in the literature, maybe due to its limited industrial application. Nevertheless, it is suitable for our purposes as we can construct three different solutions to stationary compressible Euler equations with this geometry.

Let us consider the radius (39) in an interval I given by $x_a = -0.05\,\mathrm{m}$ and $x_b = 0.55\,\mathrm{m}$ as shown in Fig. 8.

Figure 8. Geometry of the triple nozzle.

In this case, the boundary conditions are chosen as $p_a = 60000\,\mathrm{Pa}$, $\theta_a = 368.16\,\mathrm{K}$ and $p_b = 20000\,\mathrm{Pa}$. The positive value of the inlet velocity u_a is, analogously as in the previous example, computed in such a way that the nozzle works in the Laval regime. The inlet density ϱ_a is computed using (4).

The interval I is divided equidistantly into $N_{\mathrm{elem}} = 1500$ finite volumes. In Figs. 9, 10 and 11, we show three different solutions to Problem 1. Again, analytical solutions are depicted by solid lines and the steady finite volume solutions are represented by dashed lines. In Figs. 12 to 17, results of the corresponding axisymmetric computation are shown. This time, we used a structured triangular grid with 4500 elements.

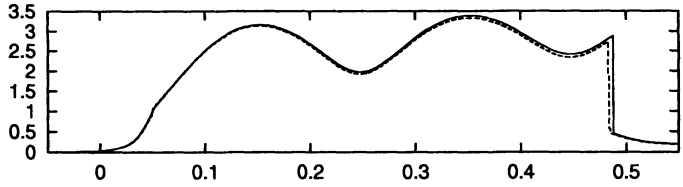

Figure 9. Mach number, quasi-one-dimensional exact (solid line) and steady finite volume (dashed line) solution with exactly one shock.

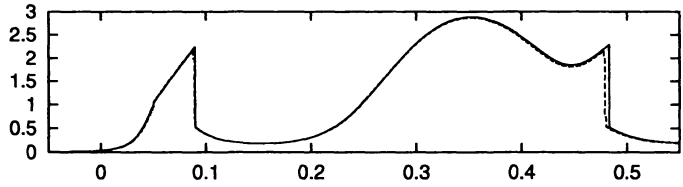

Figure 10. Mach number, quasi-one-dimensional exact (solid line) and steady finite volume (dashed line) solution with exactly two shocks.

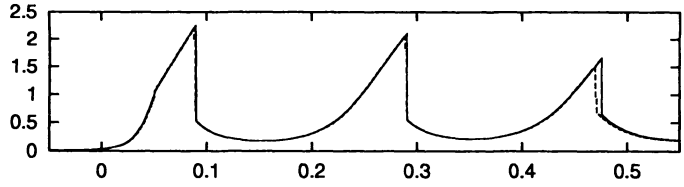

Figure 11. Mach number, quasi-one-dimensional exact (solid line) and steady finite volume (dashed line) solution with three shocks.

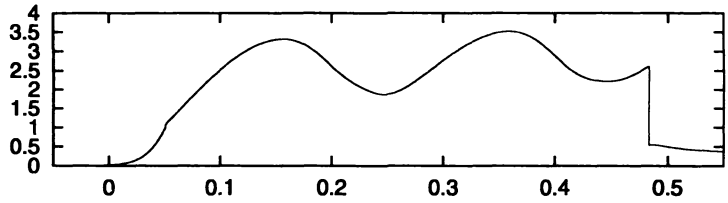

Figure 12. Mach number along the axis, steady three-dimensional axisymmetric finite volume solution with exactly one shock.

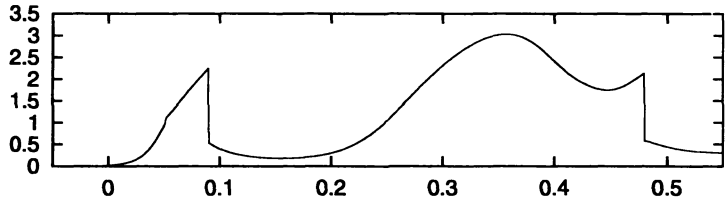

Figure 13. Mach number along the axis, steady three-dimensional axisymmetric finite volume solution with exactly two shocks.

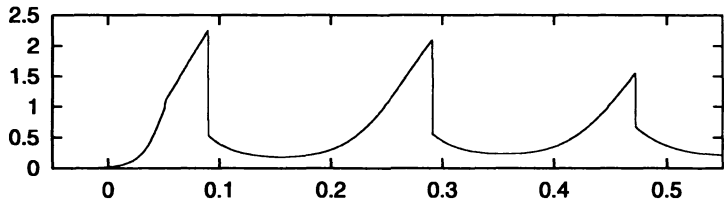

Figure 14. Mach number along the axis, steady three-dimensional axisymmetric finite volume solution with three shocks.

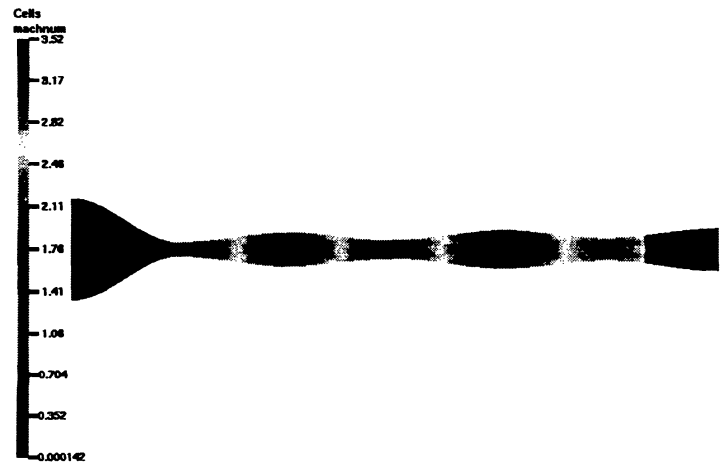

Figure 15. Mach number gray scale map, steady three-dimensional axisymmetric finite volume solution with exactly one shock.

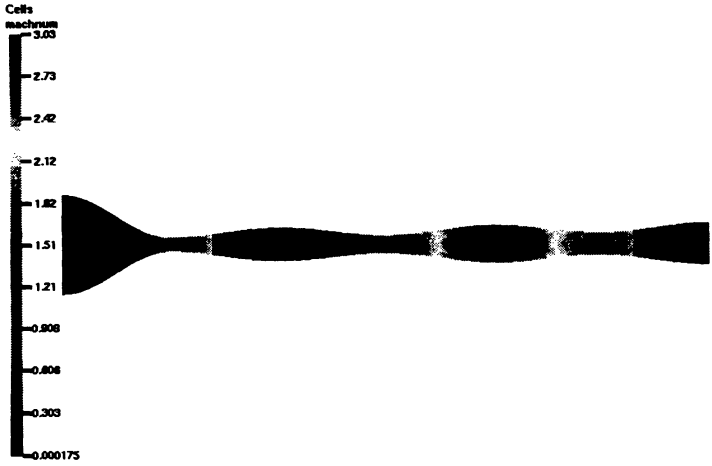

Figure 16. Mach number gray scale map, steady three-dimensional axisymmetric finite volume solution with exactly two shocks.

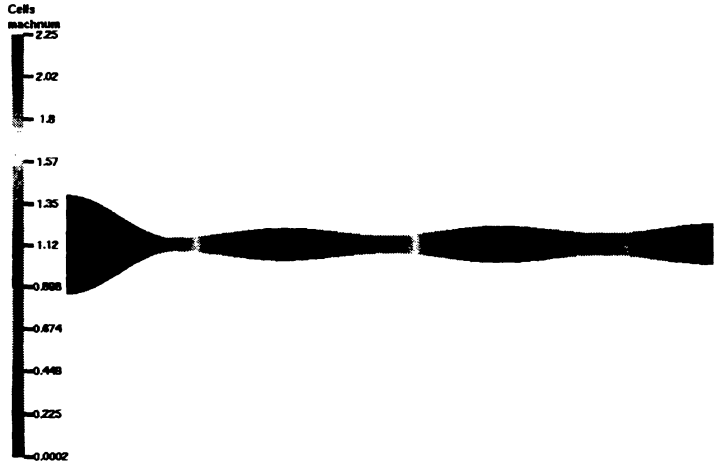

Figure 17. Mach number gray scale map, steady three-dimensional axisymmetric finite volume solution with three shocks.

In both examples, the reader can observe a good agreement between the analytical and numerical results. This means that the reason for non-uniqueness does not lie in the quasi-one-dimensional simplification of the compressible Euler equations. The presented numerical experiments document that non-uniqueness is also present in general three-dimensional equations.

References

[1] *M. Feistauer*: Mathematical Methods in Fluid Dynamics. Longman Scientific & Technical, Harlow, 1993.

[2] *J. Felcman, P. Šolín*: On the construction of the Osher-Solomon scheme for 3D Euler equations. East-West J. Numer. Math. *6* (1998), 43–64.

[3] *C. Hirsch*: Numerical Computation of Internal and External Flows, Vol. 2. J. Wiley & Sons, Chichester, 1990.

[4] *D. D. Knight*: Inviscid Compressible Flow. The Handbook of Fluid Dynamics. CRC, 1998.

[5] *L. D. Landau, E. M. Lifschitz*: Fluid Mechanics. Pergamon Press, London, 1959.

[6] *H. Ockendon, A. B. Tayler*: Inviscid Fluid Flow. Springer-Verlag, New York-Heidelberg-Berlin, 1983.

[7] *H. Ockendon, J. R. Ockendon*: The Fanno Model for Turbulent Compressible Flow. Preprint, OCIAM. Mathematical Institute, Oxford University, Oxford, 2001.

[8] *S. Osher, F. Solomon*: Upwind difference schemes for hyperbolic systems of conservation laws. Math. Comp. *38* (1982), 339–374.

[9] *A. H. Shapiro*: The Dynamics and Thermodynamics of Compressible Fluid Flow, Vol. 1. The Ronald Press Co., New York, 1953.

[10] *J. L. Steger, R. F. Warming*: Flux vector splitting of the inviscid gasdynamics equations with applications to finite-difference methods. J. Comput. Phys. *40* (1981), 263–293.

[11] *A. Terenzi, N. Mancini, F. Podenzani*: Transient Compressible Flow in Pipelines: a Godunov-type Solver for Navier-Stokes Equations. Preprint, 2000.

[12] *E. Truckenbrodt*: Fluidmechanik, Band 2. Springer-Verlag, Berlin-Heidelberg-New York, 1980.

[13] *G. Vijayasundaram*: Transonic flow simulation using upstream centered scheme of Godunov type in finite elements. J. Comput. Phys. *63* (1986), 416–433.

[14] *A. J. Ward-Smith*: Internal Fluid Flow, The Fluid Dynamics of Flow in Pipes and Ducts. Clarendon Press, Oxford, 1980.

[15] *P. Wesseling*: Principles of Computational Fluid Dynamics. Springer-Verlag, Berlin, 2000.

Authors' addresses: *P. Šolín*, CAAM, Rice University, Houston, TX 77251-1892, U.S.A., e-mail: `solin@rice.edu`; *K. Segeth*, Mathematical Institute of the Academy of Sciences of the Czech Republic, Žitná 25, 115 67 Praha 1, Czech Republic, e-mail: `segeth@math.cas.cz`.

49 (2004) APPLICATIONS OF MATHEMATICS No. 3, 247–268

NON-UNIQUENESS OF ALMOST UNIDIRECTIONAL INVISCID COMPRESSIBLE FLOW*

Pavel Šolín, Houston, Karel Segeth, Praha

(Received March 25, 2002)

Abstract. Our aim is to find roots of the non-unique behavior of gases which can be observed in certain axisymmetric nozzle geometries under special flow regimes. For this purpose, we use several versions of the compressible Euler equations. We show that the main reason for the non-uniqueness is hidden in the energy decomposition into its internal and kinetic parts, and their complementary behavior. It turns out that, at least for inviscid compressible flows, a bifurcation can occur only at flow regimes with the Mach number equal to one (sonic states). Analytical quasi-one-dimensional results are supplemented by quasi-one-dimensional and axisymmetric three-dimensional finite volume computations. Good agreement between quasi-one-dimensional and axisymmetric results, including the presence of multiple stationary solutions, is presented for axisymmetric nozzles with reasonably small slopes of the radius.

Keywords: non-uniqueness, inviscid gas flow, compressible Euler equations, quasi-one-dimensional, axisymmetric, finite volume method

MSC 2000: 35L65, 65H10, 76H05, 76M25, 76N10, 76N15

1. Introduction

The theory of almost unidirectional inviscid flow of perfect gases in tubes, ducts, pipes and nozzles is a relatively well-explored discipline (see, e.g., [3], [4], [5], [6], [7], [9], [12], [14], [15]), which deserves a permanent industrial attention. Nevertheless, only surprisingly few remarks can be found in the literature on the non-unique behavior that these flows can exhibit at sonic and transonic regimes in nontrivial

* This work was partly supported by the Grants GP 102/01/D114 and 201/04/1305 of the Grant Agency of the Czech Republic.

axisymmetric geometries. It is our aim to provide some analytical and numerical insight into this phenomenon in the present paper.

In Paragraph 2.1 we briefly recall the derivation of a basic quasi-one-dimensional model for inviscid compressible flow from the stationary quasi-one-dimensional compressible Euler equations. Attention is given to a sufficiently precise mathematical formulation. Although the model is a classical one (see, e.g., [3], [4], [5], [6], [12], [14], most analytical results are limited to *simple* and *Laval* nozzles (probably due to their predominant industrial importance), where the non-uniqueness of solution does not appear. We investigate existence of non-unique solutions in Paragraph 2.2, and present a recursive algorithm for the construction of all exact solutions in general multiple nozzles in Paragraph 2.6, using some preliminary results obtained in Paragraphs 2.3, 2.4 and 2.5.

Section 4 uses a few flow examples to compare analytical results constructed by means of the recursive algorithm from Section 2 with corresponding numerical results, computed using a quasi-one-dimensional and an axisymmetric three-dimensional finite volume schemes described in Section 3.

2. Quasi-one-dimensional model

In this section we will analyze a quite simple basic model of almost unidirectional inviscid compressible flow, which at the same time offers a sufficiently complex description of the flow and is sufficiently transparent to have an analytical solution. Obviously, for real-life industrial simulations, advanced quasi-one-dimensional models (such as, e.g., the Fanno model discussed in [4], [5], [7], [9] including wall drag and turbulence effects, or a viscous model [11]) are recommended.

2.1. Derivation of the model

Let us consider a bounded interval $I = [x_a, x_b] \subset \mathbb{R}$, real constants $0 < R_{\min} \leqslant R_{\max}$ and a bounded real function $r(x)\colon\ I \to [R_{\min}, R_{\max}]$ describing the radius of an axisymmetric pipe or nozzle. For simplicity, we assume that $r(x)$ is once continuously differentiable in (x_a, x_b) and continuous in I, but the results presented in this paper are valid also for $r(x)$ continuous and only piecewise smooth. We define a varying cross-section $a(x) = \pi r^2(x)$ for $x \in I$.

Stationary quasi-one-dimensional compressible Euler equations. The stationary quasi-one-dimensional compressible Euler equations (with the varying cross-

section a) are considered in the usual form

$$\frac{\partial a(x)\varrho(x)u(x)}{\partial x} = 0, \tag{1}$$

$$\frac{\partial a(x)[\varrho(x)u^2(x) + p(x)]}{\partial x} = p(x)\frac{\partial a(x)}{\partial x}, \tag{2}$$

$$\frac{\partial a(x)u(x)[e(x) + p(x)]}{\partial x} = 0, \tag{3}$$

$x \in (x_a, x_b)$, which can be found, e.g., in [3], [4], [5], [6], [9], [12]. Here $\varrho(x)$, $u(x)$, $p(x)$, $e(x)$ mean the density, velocity, pressure and total energy density, respectively. Total energy density e is defined as a sum of its internal and kinetic parts by the relation $e = p/(\kappa - 1) + \varrho u^2/2$, where $\kappa \in (1, 3)$ is a real constant. The flow is assumed to obey the perfect gas state equation

$$p(x) = \varrho(x)R\theta(x) \tag{4}$$

where R is the gas constant and $\theta(x)$ the absolute temperature.

Transformation of the governing equations. It is well known that, due to the hyperbolicity of the compressible Euler equations, only piecewise smooth but generally discontinuous solutions can be expected. In our case, all *discontinuities* are *shocks* (simultaneous discontinuities in all of ϱ, u and p), as contact discontinuities are not relevant (see, e.g., [15]).

Along smooth parts of the solution, (1) and (3) are equivalent to

$$a(x)\varrho(x)u(x) = m, \tag{5}$$

$$\frac{\kappa p(x)}{(\kappa - 1)\varrho(x)} + \frac{1}{2}u^2(x) = h, \tag{6}$$

where the symbols m, h are real constants denoting the mass flux and enthalpy, respectively. The Rankine-Hugoniot conditions imply that m, h are conserved also at shocks (see, e.g., [15]).

As the rate of momentum ϱu is not conserved in (2) due to a source term on the right-hand side, we usually consider the conservation of entropy

$$S(x) = c_v \ln \frac{p(x)}{\varrho^\kappa(x)} + \text{const.} \tag{7}$$

on smooth parts of the solution (see, e.g., [3], [12]). Detailed derivation of (7) and further properties of the entropy S can be found, e.g., in [1], [3], [4], [5], [6], [9], 15]. At shocks, the Rankine-Hugoniot condition

$$p(x_+) = p(x_-)\frac{2\kappa M(x_-)^2 - \kappa + 1}{\kappa + 1} \tag{8}$$

(see, e.g., [3], [12], [15]) can be used instead of (7). Here $x \in I$ and $p(x_+)$, $p(x_-)$, $M(x_-)$ mean the downstream pressure limit and the upstream pressure and the Mach number (defined below) limits at the shock, respectively.

Therefore (2) can be replaced by the conservation of the quantity

$$\frac{p(x)}{\varrho^\kappa(x)} = s \tag{9}$$

along continuous parts of the solution. Finally, let us recall the speed of sound $c(x)$ and the Mach number $M(x)$, defined by

$$c(x) = (\kappa p(x)/\varrho(x))^{1/2}, \quad M(x) = |u(x)|/c, \tag{10}$$

respectively. The flow is called *subsonic* where $M(x) < 1$, *sonic* where $M(x) = 1$ and *isentropic* where the quantity s from (9) is conserved.

Let us briefly recall some basic achievements of the fluid mechanics in the following Lemma 2.1.

Lemma 2.1. *Shocks cannot occur in subsonic or sonic flow regions. A flow leaves a shock always at subsonic regime. The entropy S and the quantity s defined in* (9) *are discontinuous at shocks and always increasing with respect to the flow direction. Both of these quantities stay conserved except for shocks.*

P r o o f. See basic literature on fluid mechanics, e.g. [1]. □

P r o b l e m 1. Let I, r, a be as described in Paragraph 2.1. Consider boundary data $\varrho_a > 0$, $u_a > 0$, $p_a > 0$, $p_b > 0$. Let us put $m = a(x_a)\varrho_a u_a$, $h = \kappa p_a/((\kappa-1)\varrho_a) + u_a^2/2$ according to (5) and (6), respectively. For a finite set $\mathcal{D} \subset (x_a, x_b)$ (corresponding to shocks), partitioning (x_a, x_b) into a finite number of non-overlapping open intervals $I_1, I_2, \ldots, I_d$ (ordered from the left to the right), we consider a sequence of constants $p_a/\varrho_a^\kappa = s_1 < s_2 < \ldots < s_d$. The set $\mathcal{D}$ and real functions ϱ, u, p defined in $I \setminus \mathcal{D}$ are sought such that

1. ϱ, u, p are bounded, positive and smooth in $I \setminus \mathcal{D}$;
2. ϱ, u, p satisfy (5), (6) in $I \setminus \mathcal{D}$ with the constants m, h, respectively;
3. ϱ, p satisfy (9) in $I \setminus \mathcal{D}$ with $p/\varrho^\kappa = s_k$ in I_k, for all $1 \leqslant k \leqslant d$;
4. ϱ, u, p satisfy (8) at all $x \in \mathcal{D}$;
5. $\varrho(x_a) = \varrho_a$, $u(x_a) = u_a$, $p(x_a) = p_a$, $p(x_b) = p_b$.

In what follows, we will solve Problem 1 instead of the original differential equations (1), (2), (3).

2.2. A model problem with a non-unique solution

Lemma 2.2. *If Problem* 1 *has a solution* ϱ, u, p, *there is a unique pair of values* $\varrho_b, u_b > 0$ *such that* $\varrho(x_b) = \varrho_b$, $u(x_b) = u_b$. *If* $p_b = p_a$, *then* $\varrho_b = \varrho_a$, $u_b = u_a$.

P r o o f. Let us assume that a solution to Problem 1 exists. Equations (5), (6), expressing the conservation of m, h in $I \setminus \mathcal{D}$, yield a quadratic equation for $u(x_b) = u_b$. It is easy to see that this equation has always one positive and one negative root. The negative one is eliminated in view of (5). Relation (5) yields also the density ϱ_b. The rest is easy to see. □

Theorem 2.1. *Let the radius* r *be as described in Paragraph* 2.1 *and moreover satisfy* $r(x_a) = r(x_b) = r_0 > 0$, $r(x) > r_0$ *for all* $x \in (x_a, x_b)$. *Let the boundary data of Problem* 1 *satisfy* $M_a = u_a/(\kappa p_a/\varrho_a)^{1/2} = 1$, $p_b = p_a$. *Then Problem* 1 *has exactly two solutions in* I, *both of them smooth in* (x_a, x_b).

P r o o f. According to Lemma 2.2, a solution of Problem 1 must satisfy $\varrho(x_b) = \varrho_a$. As $p_a/\varrho_a^\kappa = p(x_b)/\varrho^\kappa(x_b)$, Lemma 2.1 yields that $\mathcal{D} = \emptyset$. Thus, the relation (8) is not relevant. Putting (5) and (9) into (6), we obtain

$$\frac{\kappa s}{\kappa - 1}\varrho^{\kappa-1}(x) + \frac{m^2}{2a^2(x)\varrho^2(x)} - h = 0 \tag{11}$$

for all $x \in I$. For an $x \in I$, the equation (11) can be written in the form

$$f_\varrho(\varrho(x)) = 0, \tag{12}$$

with the implicit function

$$f_\varrho(\xi) = \frac{\kappa s}{\kappa - 1}\xi^{\kappa-1} + \frac{m^2}{2a^2(x)\xi^2} - h \tag{13}$$

defined for all $\xi \in (0, \infty)$. The function f_ϱ is smooth and it achieves its only minimum at

$$\xi_{\min} = \Big(\frac{m^2}{\kappa a^2(x) s}\Big)^{\frac{1}{\kappa+1}}. \tag{14}$$

The derivative f'_ϱ is negative in $(0, \xi_{\min})$ and positive in $(\xi_{\min}, \infty)$. Further, $f_\varrho(\xi_{\min}) = 0$ both for x_a and x_b. For all $x \in I$, the value of $f_\varrho(\xi_{\min})$ is a decreasing function of the cross-section $a(x)$. Thus, the equation (12) has exactly one positive root $\varrho_1(x) = \varrho_2(x) = \varrho_a$ for $x = x_a$, exactly two positive roots $0 < \varrho_1(x) < \varrho_2(x)$ for all $x \in (x_a, x_b)$ and exactly one positive root $\varrho_1(x) = \varrho_2(x) = \varrho_a$ for $x = x_b$. The implicit function theorem immediately yields that the functions $\varrho_1(x)$, $\varrho_2(x)$ are smooth in (x_a, x_b). Putting the solutions $\varrho_1(x)$, $\varrho_2(x)$ into the equation (5), we obtain two different positive smooth solutions $u_1(x)$, $u_2(x)$ for the velocity. Finally, using (9), we obtain the corresponding solutions $p_1(x)$, $p_2(x)$ for the pressure. □

Let us remark that in case of two positive roots $0 < \varrho_1(x) < \varrho_2(x)$ the Mach number $M_1(x)$ corresponding to the solution $\varrho_1(x)$, $u_1(x)$, $p_1(x)$ is greater than one, i.e. the corresponding flow state is supersonic. Analogously, the Mach number $M_2(x)$ corresponding to the solution $\varrho_2(x)$, $u_2(x)$, $p_2(x)$ is less than one and thus the corresponding flow state is subsonic.

2.3. Properties of sonic points

As we have seen in the previous paragraph, *sonic points* (points $x \in I$ such that $M(x) = 1$) play an important role in the existence of non-unique solutions to Problem 1. It is our aim to mention some of their further useful properties in this paragraph.

Lemma 2.3. *Let $\mathcal{D}, \varrho, u, p$ solve Problem* 1. *Let $x \in I \setminus \mathcal{D}$ be such that $M(x) = 1$. Then the solution of Problem* 1 *at x has the unique form*

$$
\begin{aligned}
u(x) &= \Big(\frac{2h(\kappa-1)}{\kappa+1}\Big)^{1/2}, \\
\varrho(x) &= \frac{m}{a(x)u(x)}, \\
p(x) &= \frac{(\kappa-1)\varrho(x)[h - u^2(x)/2]}{\kappa}.
\end{aligned} \tag{15}
$$

P r o o f. Immediate from (5), (6) using (10). □

Lemma 2.4. *Let $\mathcal{D}$, ϱ, u, p solve Problem* 1. *Let $x_1, x_2 \in I \setminus \mathcal{D}$, $x_1 < x_2$, $M(x_1) = M(x_2) = 1$ and $a(x_1) = a(x_2)$. Then ϱ, u, p are continuous in $[x_1, x_2]$.*

P r o o f. Using Lemma 2.3 with $a(x_1) = a(x_2)$, we obtain $\varrho(x_1) = \varrho(x_2)$, $p(x_1) = p(x_2)$. Thus, $p(x_1)/\varrho^\kappa(x_1) = p(x_2)/\varrho^\kappa(x_2)$. Lemma 2.1 implies the continuity of ϱ, u, p in $[x_1, x_2]$. This obviously means that there is no $\tilde{x} \in \mathcal{D}$, $x_1 < \tilde{x} < x_2$. □

Lemma 2.5. *Let $\mathcal{D}, \varrho, u, p$ solve Problem* 1. *Let $x_1, x_2 \in I \setminus \mathcal{D}$, $x_1 < x_2$, $M(x_1) = M(x_2) = 1$ and $a(x_1) \neq a(x_2)$. Then none of ϱ, u, p can be continuous in $[x_1, x_2]$. Moreover, necessarily it is $a(x_1) < a(x_2)$.*

P r o o f. Lemma 2.3 with $a(x_1) \neq a(x_2)$ yields that $\varrho(x_1) \neq \varrho(x_2)$, $p(x_1) \neq p(x_2)$. This and the conservation of m, h in $I \setminus \mathcal{D}$ yield that $p(x_1)/\varrho^\kappa(x_1) \neq p(x_2)/\varrho^\kappa(x_2)$. Lemma 2.1 implies that $p(x_1)/\varrho^\kappa(x_1) < p(x_2)/\varrho^\kappa(x_2)$. Relation (15) yields that this is only possible if $a(x_1) < a(x_2)$. □

Lemma 2.6. *Let $\mathcal{D}$, ϱ, u, p solve Problem* 1. *Let $x_1, x_2 \in I \setminus \mathcal{D}$, $x_1 < x_2$, and let ϱ, u, p be continuous in $[x_1, x_2]$.*

a) *If $M(x_1) < 1$ and $r(x)$ is decreasing in $[x_1, x_2]$ then $M(x)$ is increasing in $[x_1, x_2]$, but the relation $M(x) < 1$ is preserved in $[x_1, x_2)$.*

b) *If $M(x_1) < 1$ and $r(x)$ is increasing in $[x_1, x_2]$ then $M(x)$ is decreasing in $[x_1, x_2]$, and obviously $M(x) < 1$ in $[x_1, x_2]$.*

c) *If $M(x_1) > 1$ and $r(x)$ is decreasing in $[x_1, x_2]$ then $M(x)$ is decreasing in $[x_1, x_2]$, but the relation $M(x) > 1$ is preserved in $[x_1, x_2)$.*

d) *If $M(x_1) > 1$ and $r(x)$ is increasing in $[x_1, x_2]$ then $M(x)$ is increasing in $[x_1, x_2]$, and obviously $M(x) > 1$ in $[x_1, x_2]$.*

P r o o f. We put $s_1 = p(x_1)/\varrho^\kappa(x_1)$. Let $x \in (x_1, x_2)$. For ϱ, u, p continuous, the relations (5), (6) and (9) with (10) yield

$$u^2(x) = \frac{2(\kappa-1)h}{2/M^2(x) + \kappa - 1}, \tag{16}$$

$$\varrho(x) = \frac{m}{a(x)u(x)}, \tag{17}$$

$$s_1 = \frac{a^{\kappa-1}(x)(2(\kappa-1)h)^{(\kappa+1)/2}}{\kappa m^{\kappa-1} M^2(x)[2/M^2(x) + \kappa - 1]^{(\kappa+1)/2}}. \tag{18}$$

Relation (18) can be written as

$$M^2(x)(2/M^2(x) + \kappa - 1)^{(\kappa+1)/2} \frac{1}{a^{\kappa-1}(x)} = \frac{(2(\kappa-1)h)^{(\kappa+1)/2}}{\kappa m^{\kappa-1} s_1} = \text{const}. \tag{19}$$

We consider (19) as an implicit function for the Mach number M. An analysis of the shape of its solution (taking into account the monotonicity of r supposed in a) to d)) yields the monotone behavior of M. This analysis also yields that in a) and c), the existence of an $x \in (x_1, x_2)$ such that $M(x) = 1$ is contradictory to (19). □

Corollary 2.1. *Without loss of generality, we can assume that $M(x_a) \neq 1$ if the radius r does not have a local minimum at x_a (namely, using the implicit function f_ϱ from the proof of Theorem* 2.1, *it can be shown that there would be no solution to Problem* 1*). Thus, Lemma* 2.6 *excludes all possibilities for the existence of sonic points except for such $x \in I$ where the radius r achieves a local minimum.*

Corollary 2.1 together with Lemma 2.3 will play an important role in the construction of multiple solutions as we will be able to evaluate solution of Problem 1 at these points in the pipe or nozzle a priori. Now let us turn our attention to the solution of Problem 1. For the sake of simplicity, we will deal with two simplified situations

in Paragraphs 2.4 and 2.5 first. A general recursive algorithm will be designed in Paragraph 2.6.

2.4. Isentropic solutions to Problem 1

In this paragraph we will discuss existence of isentropic solutions to Problem 1 (i.e. solutions satisfying $\mathcal{D} = \emptyset$) and construct all of them if relevant.

Lemma 2.2 allows us to compute values $\varrho_b, u_b > 0$ such that the boundary conditions $\varrho(x_b) = \varrho_b$, $u(x_b) = u_b$ are satisfied by all solutions to Problem 1. We put

$$s = \frac{p_a}{\varrho_a^\kappa}, \quad s_b = \frac{p_b}{\varrho_b^\kappa}. \tag{20}$$

An isentropic solution to Problem 1 can exist only if $s = s_b$. In this case we proceed analogously as in the proof of Theorem 2.1. Equation (8) is not relevant and (5), (6), (9) yield (11). There is an isentropic solution to Problem 1 if (12) has at least one real root for all $x \in I$, i.e. if

$$f_\varrho(\xi_{\min}) \leqslant 0 \tag{21}$$

for all $x \in I$. It is easy to see that the value of $f_\varrho(\xi_{\min})$ is a decreasing function of the radius r. Therefore it is sufficient to verify the condition (21) only at the global minimum of r in I. All isentropic solutions to Problem 1 are constructed using all real roots of (12) in the whole interval I as described in the algorithm below. It is not difficult to see that nonunique continuous solutions appear only in the situation described in Theorem 2.1.

Algorithm for the construction of all isentropic solutions.

- Verify the necessary condition $s(x_1) = s(x_2)$ for the existence of an isentropic solution.
- Verify the sufficient and necessary condition (21) for the existence of an isentropic solution at the point y_{i_0} where the global minimum of r in $[x_1, x_2]$ is achieved.
- If an isentropic solution exists, cover the interval $[x_1, x_2]$ with a sufficiently fine equidistant partition $x_1 = y_1 < y_2 < \ldots < y_{N_0} = x_2$.
- For $i := 1, 2, \ldots, N_0 - 1$ do
  - Compute all real roots of the equation (12) at y_i. If there is exactly one real root, it has the meaning of a sonic density at y_i. If there are two real roots, they have the meaning of the subsonic and the supersonic (in the sense of the remark at the end of Paragraph 2.2) density at the point y_i.
  - For all real roots at y_i obtained in the previous step compute the pressure $p(y_i)$ and the velocity $u(y_i)$ to get a complete flow state (states) at y_i.

With a sufficiently fine partition of the interval $[x_1, x_2]$, the algorithm finds all isentropic solutions connecting the states at x_1 and x_2.

2.5. Solutions to Problem 1 with exactly one shock

Now let us discuss the existence of solutions to Problem 1 which contain exactly one shock ($\mathrm{card}(\mathcal{D}) = 1$) and construct all of them if relevant.

Analogously as in the previous case, Lemma 2.2 allows us to compute values $\varrho_b, u_b > 0$ such that the boundary conditions $\varrho(x_b) = \varrho_b$, $u(x_b) = u_b$ are satisfied by all solutions to Problem 1. We put

$$s = \frac{p_a}{\varrho_a^\kappa}, \quad s_b = \frac{p_b}{\varrho_b^\kappa}. \tag{22}$$

Problem 1 can have a solution containing exactly one shock only if $s < s_b$. Suppose that the one shock case occurs and let $\tilde{x} \in (x_a, x_b)$ be the position of the discontinuity. We put $\varrho_L = \varrho(\tilde{x}_-)$, $u_L = u(\tilde{x}_-)$, $p_L = p(\tilde{x}_-)$, $\varrho_R = \varrho(\tilde{x}_+)$, $u_R = u(\tilde{x}_+)$, $p_R = p(\tilde{x}_+)$. Solutions of Problem 1 with exactly one shock at $\tilde{x}$ must satisfy the following three conditions:

1. Equations (5), (6), (9) with the boundary data $\varrho(x_a) = \varrho_a$, $u(x_a) = u_a$, $p(x_a) = p_a$, $\varrho(\tilde{x}_-) = \varrho_L$, $u(\tilde{x}_-) = u_L$, $p(\tilde{x}_-) = p_L$ are satisfied in $[x_a, \tilde{x})$.
2. Equations (5), (6), (9) with the boundary data $\varrho(\tilde{x}_+) = \varrho_R$, $u(\tilde{x}_+) = u_R$, $p(\tilde{x}_+) = p_R$, $\varrho(x_b) = \varrho_b$, $u(x_b) = u_b$, $p(x_b) = p_b$ are satisfied in $(\tilde{x}, x_b]$.
3. Values $p(\tilde{x}_-)$, $p(\tilde{x}_+)$ and $M(x_+) = |u(x_+)|/(\kappa p(x_+)/\varrho(x_+))^{1/2}$ satisfy the Rankine-Hugoniot relation (8).

The reader may note that isentropic solutions in $[x_a, \tilde{x})$ and $(\tilde{x}, x_b]$, required in items 1 and 2, need not be unique if geometrical situation from Theorem 2.1 occurs. Conditions 1 to 3 can be translated into the following system of nonlinear algebraic equations

$$\frac{\kappa p_L}{(\kappa - 1)(p_L/s)^{1/\kappa}} + \frac{m^2}{2a^2(\tilde{x})(p_L/s)^{2/\kappa}} - h = 0, \tag{23}$$

$$\frac{\kappa p_R}{(\kappa - 1)(p_R/s_b)^{1/\kappa}} + \frac{m^2}{2a^2(\tilde{x})(p_R/s_b)^{2/\kappa}} - h = 0, \tag{24}$$

$$\mathcal{R}(p_L, p_R) = p_R - \frac{2m^2(s/p_L)^{1/\kappa}/a^2(\tilde{x}) - (\kappa - 1)p_L}{\kappa + 1} = 0 \tag{25}$$

for unknowns $\tilde{x}$, p_L, p_R. Here $\mathcal{R}$ is a residuum of the Rankine-Hugoniot relation (8). The equation (25) is solved iteratively, using a sufficiently fine equidistant partition of I for initial guesses of $\tilde{x}$ and nested iterative procedures for the solution of (23), (24).

Algorithm for the construction of solutions with exactly one shock

- Verify the necessary condition $s(x_1) < s(x_2)$ for existence of a solution with exactly one shock.
- If the previous verification was successful, cover the interval $[x_1, x_2]$ with a sufficiently fine equidistant partition $x_1 = y_1 < y_2 < \ldots < y_{N_1} = x_2$.
- For $i := 1, 2, \ldots, N_1 - 1$ do
  - Compute the supersonic roots (in the sense of the remark in the end of Paragraph 2.2) of the equation (23) at the points y_i, y_{i+1} and denote them by $\tilde{p}_{L_1}$, $\tilde{p}_{L_2}$, respectively.
  - Compute the subsonic roots of the equation (24) at y_i, y_{i+1} and denote them by $\tilde{p}_{R_1}$, $\tilde{p}_{R_2}$, respectively.
  - Compute the values $\mathcal{R}(\tilde{p}_{L_1}, \tilde{p}_{R_1})$, $\mathcal{R}(\tilde{p}_{L_2}, \tilde{p}_{R_2})$ from (25). If their signs differ, resolve the value of $\tilde{x} \in [y_i, y_{i+1}]$ by means of the interval bisection method with a sufficient accuracy. In our code we use 10^{-10}.
  - Compute the density and the velocity ϱ_L, u_L and ϱ_R, u_R at $\tilde{x}$ using the obtained values of p_L, p_R, respectively, and the values of m, h.
  - Verify that the state ϱ_1, u_1, p_1 at x_1 can be isentropically connected with the state ϱ_L, u_L, p_L at $\tilde{x}$ and find all possible connections as described in Paragraph 2.4.
  - Verify that the state ϱ_R, u_R, p_R at $\tilde{x}$ can be isentropically connected with the state ϱ_2, u_2, p_2 at x_2 and find all possible connections as described in Paragraph 2.4.

With a sufficiently fine partition of the interval $[x_1, x_2]$, the algorithm finds all single shock solutions connecting the states at x_1 and x_2.

2.6. Algorithm for the construction of all solutions to Problem 1

Finally, we can introduce a recursive algorithm for the construction of all solutions to Problem 1 in this paragraph.

Analogously as in Paragraphs 2.4 and 2.5, Lemma 2.2 allows us to compute values $\varrho_b, u_b > 0$ such that boundary conditions $\varrho(x_b) = \varrho_b$, $u(x_b) = u_b$ are satisfied by all solutions to Problem 1. We put

$$s = \frac{p_a}{\varrho_a^\kappa}, \quad s_b = \frac{p_b}{\varrho_b^\kappa}. \tag{26}$$

If $s > s_b$, there is no solution to Problem 1 due to Lemma 2.1. If $s = s_b$, there can be only isentropic solutions to Problem 1. We use the algorithm designed in Paragraph 2.4. If $s < s_b$, we can expect only discontinuous solutions. All solutions to Problem 1 containing exactly one shock are constructed as shown in Paragraph 2.5.

Before we start constructing solutions with multiple shocks, it is natural to ask how many of them can be expected.

Lemma 2.7. *Let $I_0 = [x_1, x_2] \subset I$ and r be constant in I_0. Let Problem 1 have a solution. If the solution is subsonic or sonic in I_0, it is necessarily constant in I_0. If $M(x_1) > 1$, the solution is either constant in I_0 or piecewise constant with exactly one shock in I_0. In the case of shock, the solution of Problem 1 is not unique because all shock positions $x_s \in I_0$ are possible.*

P r o o f. In the subsonic or sonic case, no shock occurs due to Lemma 2.1. Using (5), (6), (9) and $r = \text{const.}$ in I_0, we obtain that ϱ, u, p can be only constant in I_0. If $M(x_1) > 1$ and no shock occurs, the solution is constant for the same reason as before. If there is a shock (at most one due to Lemma 2.1) at an $x_s \in I_0$, (5), (6), (9) are conserved in both intervals $[x_1, x_s)$, $(x_s, x_2]$, obviously with different constants $0 < s_1 < s_2$ in (9), respectively. There is no preferred position for the shock with respect to solvability of Problem 1. □

Estimation of the maximal number of shocks. Let us consider all local minima of the radius r, except for the endpoints x_a, x_b (if relevant), and collect them into a set

$$\mathcal{P} = \{P_1, P_2, \dots, P_N\} \subset I. \tag{27}$$

If this minimum is not unique due to a constant radius section $I_0 \subset I$, we can identify the corresponding $x \in \mathcal{P}$ with I_0 in the sense of Lemma 2.7. According to Corollary 2.1, $M(x) = 1$ can occur only if $x \in \mathcal{P}$. Lemma 2.1 yields that the maximal number of shocks in the pipe or nozzle is $N_{\max} = N$ if the inlet is subsonic and $N_{\max} = N + 1$ if the inlet is supersonic.

Construction of solutions to Problem 1 with at least two shocks. We construct all solutions to Problem 1 with more than one shock using the following recursive algorithm:

- First we find all solutions to Problem 1 containing exactly two shocks, using all candidates for sonic points from $\mathcal{P}$: for all $i := 1, 2, \dots, N$ do
  - Put $M(P_i) = 1$.
  - Compute the solution $\varrho_i = \varrho(P_i)$, $u_i = u(P_i)$, $p_i = p(P_i)$ of Problem 1 at P_i using Lemma 2.3.
  - Consider Problem $1^{1,i}$ which is a subproblem of Problem 1 in the interval $I^{1,i} = [x_a, P_i]$, with boundary conditions $\varrho(x_a) = \varrho_a$, $u(x_a) = u_a$, $p(x_a) = p_a$, $p(P_i) = p_i$.
  - Consider Problem $1^{2,i}$ which is also a subproblem of Problem 1 in the interval $I^{2,i} = [P_i, x_b]$, with boundary conditions $\varrho(P_i) = \varrho_i$, $u(P_i) = u_i$, $p(P_i) = p_i$, $p(x_b) = p_b$.

- Find all solutions containing exactly one shock to both Problem $1^{1,i}$ and Problem $1^{2,i}$, using the algorithm designed in Paragraph 2.5.
- Construct all solutions to Problem 1 as all pairs $[\mathcal{S}^{1,i}, \mathcal{S}^{2,i}]$, where $\mathcal{S}^{1,i}$ solves Problem $1^{1,i}$ and $\mathcal{S}^{2,i}$ solves Problem $1^{2,i}$.

- Analogously find all solutions containing $k = 3, 4, \ldots, N_{\max}$ shocks: Put $M(P_j) = 1$ for all subsets of $\mathcal{P}$ containing exactly $k-1$ elements. For each of these subsets, interval I is partitioned into k subintervals where k subproblems to Problem 1 are defined. To each of these subproblems, all solutions containing exactly one shock are constructed using the algorithm from Paragraph 2.5. Let us remark that some combinations of these subproblems can be excluded a priori in the sense of Lemmas 2.4 and 2.5. Finally, we merge the solutions of the subproblems analogously as in the previous case of exactly two shocks.

Let us remark that for quasi-one-dimensional geometries with several local minima of the radius r, there may be a considerable number of solutions due to the large number of combinations of the sonic points P_i. Discontinuous solutions contain stable as well as unstable shocks. It can be shown that the stable ones occur only in divergent parts of the pipe or nozzle while those positioned within convergent parts are unstable. Diagrams of the dependence of the number and positions of stable and unstable shocks on the boundary conditions turn out to have a very interesting structure. This work is currently under development.

3. Brief description of numerical schemes

Both the quasi-one-dimensional and axisymmetric three-dimensional compressible Euler equations are nonconservative, and therefore difficult to discretize by standard finite volume schemes. Thus, we briefly describe a quasi-one-dimensional scheme and develop a suitable version of the axisymmetric three-dimensional finite volume method in this section. Readers who are not familiar with the finite volume discretization of the compressible Euler equations are kindly asked to look into a book or a paper, e.g. [2], [8], [13].

Quasi-one-dimensional finite volume method. This version of the finite volume method is similar to the purely one-dimensional one. Nonconservativity of the quasi-one-dimensional compressible Euler equations can be overcome taking into account numerical flux through solid walls of the pipe or nozzle. This can be done in the same way as in three-dimensionsional finite volume schemes. Obviously, variable cross-section a is used instead of the unit one in the purely one-dimensional scheme.

Axisymmetric finite volume method. One possible way to derive an axisymmetric finite volume scheme is to start directly from the axisymmetric compressible Euler equations. However, source terms appearing on their right-hand side are a source

of considerable difficulties and numerical errors. Therefore we decided to propose another approach, which is not frequently mentioned in the literature and which significantly reduces nonconservativity problems. We start from the three-dimensional compressible Euler equations, discretize them by a three-dimensional finite volume scheme, and apply the axisymmetry of the problem to the discretized problem.

Let us consider a two-dimensional domain Ω defined by

$$\Omega = \{[x, y] \in \mathbb{R}^2;\ x \in (x_a, x_b),\ y \in (0, r(x))\} \tag{28}$$

and cover it with a standard unstructured finite element triangulation

$$\tau_h = \{T_1, T_2, \ldots, T_M\}. \tag{29}$$

By $K(i)$ we denote the set of indices of triangles $T_j \in \tau_h$, $j = 1, 2, \ldots, M$, $j \neq i$, which have a common side with the triangle $T_i \in \tau_h$, $i = 1, 2, \ldots, M$.

Let us consider an angle $\varphi \in [0, 2\pi)$ and the plane Σ constructed by the rotation of the (x, y) plane around its x-axis by the angle φ. This rotation defines a new Cartesian coordinate system $(\tilde{x}, \tilde{y}, \tilde{z})$, where $\tilde{x} \equiv x$ and the plane Σ is identical with the plane $(\tilde{x}, \tilde{y})$.

We consider a velocity vector $\boldsymbol{u} = (u_x, u_y, u_z)^T$ parallel to the plane Σ. In the new coordinate system, $\boldsymbol{u}$ can be expressed as $\tilde{\boldsymbol{u}} = (\tilde{u}_x, \tilde{u}_r, 0)^T$ with $u_y = \tilde{u}_r \cos\varphi$, $u_z = \tilde{u}_r \sin\varphi$. The rotation matrix $\overline{\mathcal{Q}}$ transforming vectors from the new coordinate system to the original one has the form

$$\overline{\mathcal{Q}} = \begin{pmatrix} 1 & 0 & 0 \\ 0 & \cos\varphi & -\sin\varphi \\ 0 & \sin\varphi & \cos\varphi \end{pmatrix}. \tag{30}$$

Obviously $\boldsymbol{u} = \overline{\mathcal{Q}}\tilde{\boldsymbol{u}}$ and $\overline{\mathcal{Q}}\overline{\mathcal{Q}}^T = I$. Conservation state vectors $\boldsymbol{w} = (\varrho, \varrho u_x, \varrho u_y, \varrho u_z, e)^T$ (ϱ and e mean the fluid density and total energy density, respectively) such that the corresponding velocity vector $\boldsymbol{u} = (u_x, u_y, u_z)^T$ is parallel to Σ, can be expressed in the new coordinate system as $\tilde{\boldsymbol{w}} = (\varrho, \varrho\tilde{u}_x, \varrho\tilde{u}_r, 0, e)^T$. The transformation matrix $\mathcal{Q} \in \mathbb{R}^5 \times \mathbb{R}^5$ defined by

$$\mathcal{Q} = \begin{pmatrix} 1 & 0 & 0 \\ 0 & \overline{\mathcal{Q}} & 0 \\ 0 & 0 & 1 \end{pmatrix}, \tag{31}$$

where 0 may denote also a zero row or column vector, transforms state vectors from the new coordinate system to the original one. Obviously, $\boldsymbol{w} = \mathcal{Q}\tilde{\boldsymbol{w}}$.

The angular flux $\boldsymbol{f}_\varphi$ has the form $\boldsymbol{f}_\varphi(\boldsymbol{w}) = -p(\boldsymbol{w})(0,0,\sin\varphi,-\cos\varphi,0)^T$ for conservation states $\boldsymbol{w}$ with velocity vectors parallel to the plane Σ. The function $p(\boldsymbol{w})$ expressing the pressure corresponding to a conservation state $\boldsymbol{w}$ has the form $p(\boldsymbol{w}) = (\kappa-1)(w_3-(w_2^2+w_3^2+w_4^2)/(2w_1))$. We will need the angular derivative of $\boldsymbol{f}_\varphi$, which has the form

$$\frac{\partial}{\partial\varphi}\boldsymbol{f}_\varphi(\boldsymbol{w}) = -p(\boldsymbol{w})(0,0,\cos\varphi,\sin\varphi,0)^T = -p(\boldsymbol{w})\mathcal{Q}(0,0,1,0,0)^T. \tag{32}$$

Now we can proceed to the finite volume method: Each triangle $T_i \in \tau_h$ represents a three-dimensional axisymmetric ring

$$R_i = \{[x,y,z] \in \mathbb{R}^3,\ x = \overline{x},\ y = \overline{y}\sin\psi,\ z = \overline{y}\cos\psi,\ [\overline{x},\overline{y}] \in T_i,\ 0 \leqslant \psi < 2\pi\}. \tag{33}$$

By $|R_i|$ we denote the volume of the ring R_i. We put $S_{ij} = \overline{R}_i \cap \overline{R}_j$, $1 \leqslant i \leqslant M$, $j \in K(i)$, $j \neq i$ and by $|S_{ij}|$ denote the surface size of S_{ij}. By $R_i(\Delta\varphi)$ we denote a segment of the ring R_i of a small angular width $\Delta\varphi > 0$, lying between the angles $\varphi - \Delta\varphi/2$, $\varphi + \Delta\varphi/2$. The corresponding section of the surface S_{ij} will be denoted by $S_{ij}(\Delta\varphi)$.

Let us consider two time-dependent conservation state vectors $\boldsymbol{w}_i(t), \boldsymbol{w}_j(t) \in \mathbb{R}^5$ corresponding to segments $R_i(\Delta\varphi)$, $R_j(\Delta\varphi)$, a normal vector ν_{ij} to $S_{ij}(\Delta\varphi)$ lying in Σ, and a standard three-dimensional numerical flux $H(\boldsymbol{w}_i(t), \boldsymbol{w}_j(t), \nu_{ij})\colon\ \mathbb{R}^5 \times \mathbb{R}^5 \times \mathbb{R}^3 \to \mathbb{R}^5$ (see, e.g., [2], [1] for its definition and properties). With $\boldsymbol{w}(t) = \mathcal{Q}\tilde{\boldsymbol{w}}(t)$, $\nu_{ij} = \overline{\mathcal{Q}}\tilde{\nu}_{ij}$ we can transform the numerical flux H into the new coordinates using its *rotational invariance* as follows,

$$H(\boldsymbol{w}_i(t), \boldsymbol{w}_j(t), \nu_{ij}) = H(\mathcal{Q}\tilde{\boldsymbol{w}}_i(t), \mathcal{Q}\tilde{\boldsymbol{w}}_j(t), \overline{\boldsymbol{Q}}\tilde{\nu}_{ij}) = \mathcal{Q}H(\tilde{\boldsymbol{w}}_i(t), \tilde{\boldsymbol{w}}_j(t), \tilde{\nu}_{ij}). \tag{34}$$

Semi-discretizing the three-dimensional compressible Euler equations in space over the segment $R_i(\Delta\varphi)$, we obtain

$$\begin{aligned}\frac{\Delta\varphi}{2\pi}|R_i|\dot{\boldsymbol{w}}_i(t) + \sum_{j\in K(i)} \frac{\Delta\varphi}{2\pi}|S_{ij}|H(\boldsymbol{w}_i(t), \boldsymbol{w}_j(t), \nu_{ij}) \\ + |T_i|(\boldsymbol{f}_{\varphi+\Delta\varphi/2}(\boldsymbol{w}_i(t)) - \boldsymbol{f}_{\varphi-\Delta\varphi/2}(\boldsymbol{w}_i(t))) = 0,\end{aligned} \tag{35}$$

where $|T_i|$ is the area of the triangle $T_i \in \tau_h$. The second term in (35) corresponds to surface sections $S_{ij}(\Delta\varphi)$ of the segment $R_i(\Delta\varphi)$, $j \in K(i)$, and the last term on the left-hand side to the angular fluxes through the segment $R_i(\Delta\varphi)$.

Expressing the state vectors $\boldsymbol{w}_i(t)$, $\boldsymbol{w}_j(t)$ in the new coordinate system, using the property $\mathcal{Q}\mathcal{Q}^T = I$, passing to the limit

$$\lim_{\Delta\varphi\to 0} \frac{\boldsymbol{f}_{\varphi+\Delta\varphi/2}(\boldsymbol{w}_i(t)) - \boldsymbol{f}_{\varphi-\Delta\varphi/2}(\boldsymbol{w}_i(t))}{\Delta\varphi} = \frac{\partial}{\partial\varphi}\boldsymbol{f}_\varphi(\boldsymbol{w}_i(t)) \tag{36}$$

and using (32), we finally obtain

$$\dot{\tilde{\boldsymbol{w}}}_i(t) = -\frac{1}{|R_i|}\sum_{j\in K(i)} |S_{ij}| H(\tilde{\boldsymbol{w}}_i(t), \tilde{\boldsymbol{w}}_j(t), \tilde{\nu}_{ij}) + \frac{2\pi|T_i|}{|R_i|} p(\tilde{\boldsymbol{w}}_i(t))(0,0,1,0,0)^T. \tag{37}$$

As the fourth component of all vectors in (37) is zero, (37) represents a two-dimensional finite volume method. Note that this axisymmetric scheme is similar to the standard two-dimensional one (see, e.g., [2], [1], [13]), using the ring volume $|R_i|$ and the common surface section size $|S_{ij}|$ where the triangle size $|T_i|$ and the common edge size $|\Gamma_{ij}|$ are used in the purely two-dimensional scheme, respectively. Moreover, an additional nonconservative pressure term

$$\frac{2\pi|T_i|}{|R_i|} p(\tilde{\boldsymbol{w}}_i(t))(0,0,1,0,0)^T, \tag{38}$$

which is not necessary in the purely two-dimensional scheme, must be used in (37).

4. Numerical examples

In this section we will present a few examples of multiple solutions in simpler quasi-one-dimensional geometries. First let us give some background for the finite volume computations which will be performed using the quasi-1D and axisymmetric schemes described in Section 3.

In Paragraphs 2.4, 2.5 and 2.6 the reader saw that all exact solutions in the quasi-1D case can be computed in a straitforward way using a sufficiently fine division of the interval I. It is also not difficult to compute *some* of the multiple solutions numerically. In such case, one only needs to choose an arbitrary admissible initial condition and the finite volume scheme converges to one of the multiple solutions. However, the situation is much more complicated if we decide to compute *all* of the multiple solutions numerically.

The task to design the initial and boundary conditions for a compressible flow computation in such a way that the resulting stationary state matches a prescribed steady solution is an extremely difficult nonlinear inverse problem that (at least up to our best knowledge) has not yet been solved. Therefore we must satisfy ourselves with a simpler approach based on the solution of direct problems with the variation of the initial condition and application of time-dependent boundary conditions.

In our case, as the computational geometries are relatively simple, it will be sufficient to use time-independent boundary conditions matching those corresponding to

the exact solution. The choice of the initial conditions is more delicate. One possible way how to construct them is to make sure that they lie sufficiently close to the exact quasi-1D (time-independent) solution. Otherwise one can often observe that the finite volume method tends to switch over to a different candidate from the set of multiple solutions, typically to a solution with a lower energy.

For all quasi-1D as well as axisymmetric finite volume computations presented in this section, the initial condition was chosen as piecewise constant by averaging the exact quasi-1D solution in the axisymmetric sense over a suitably chosen coarse subdivision of the interval I. In case of the double nozzle (Paragraph 4.1) we used 20 equally long subelements. Thirty equally long subelements were used for the triple nozzle in Paragraph 2.4.

In both following paragraphs we will use the function

$$r(x) = \begin{cases} -\dfrac{\cos(10\pi(x-0.05))}{50} + 0.0265, & x \in [x_a, 0.05], \\ -\dfrac{\sin(10\pi x)}{250} + x/100 + 1/100, & x \in [0.05, x_b] \end{cases} \tag{39}$$

with $x_a < 0.05 < x_b$ for the definition of the radius of a nozzle.

4.1. A double nozzle

We have chosen this device as it is possible to find some discussions on its behavior in the literature (see, e.g., [3], [12]). Nevertheless, those discussions are mostly based on experimental experience. The device is called a *double nozzle* as the radius r has two local minima in the interval of interest (see Fig. 1). In this case we choose $I = [x_a, x_b]$ with $x_a = -0.05\,\mathrm{m}$, $x_b = 0.35\,\mathrm{m}$.

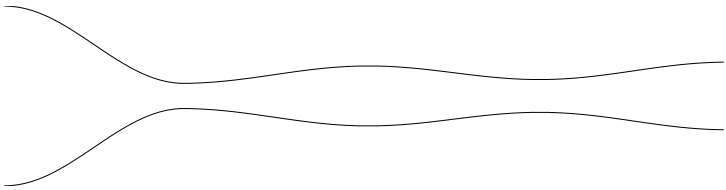

Figure 1. Geometry of the double nozzle.

We assume that the reservoir on the left-hand side is filled with almost quiet air of pressure $p_a = 50000\,\mathrm{Pa}$ and temperature $\theta_a = 368.16\,\mathrm{K}$. We choose a value $p_b = 15000$ Pa for the outer pressure. The positive inlet velocity u_a is computed in such a way that the nozzle works in the Laval regime. This regime describes free reservoir outflow with a maximal mass flux and is of crucial practical importance (see, e.g., [3], [12]. The density ϱ_a is computed from (4). In the Laval regime, the flow is sonic at such $x \in I$ where the radius r achieves its global minimum in I.

The interval I is covered with an equidistant partition of $N_{\text{elem}} = 1000$ finite volumes. In Figs. 2 and 3, two different analytical solutions to Problem 1 (obtained as described in Paragraph 2.6) are drawn by solid lines, while dashed lines represent always the corresponding steady solution of the quasi-one-dimensional finite volume scheme discussed in Section 3. In Figs. 4, 5, 6 and 7 we present steady results obtained with the axisymmetric scheme described in Section 3, corresponding to a structured triangular grid with 3000 elements.

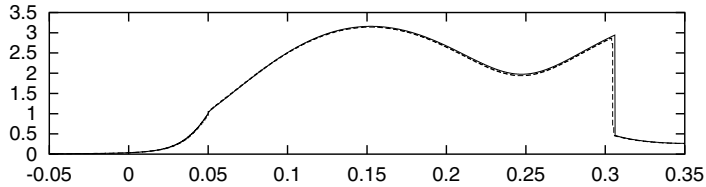

Figure 2. Mach number, quasi-one-dimensional exact (solid line) and steady finite volume (dashed line) solution with exactly one shock.

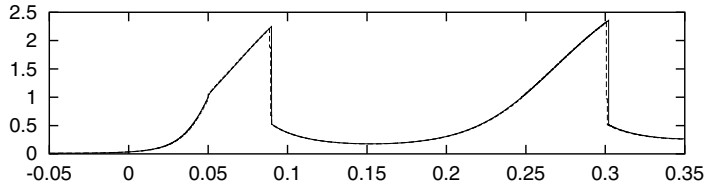

Figure 3. Mach number, quasi-one-dimensional exact (solid line) and steady finite volume (dashed line) solution with two shocks.

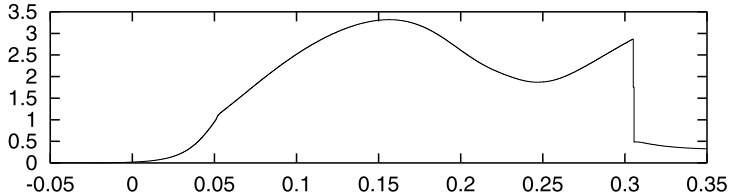

Figure 4. Mach number along the axis, steady three-dimensional axisymmetric finite volume solution with exactly one shock.

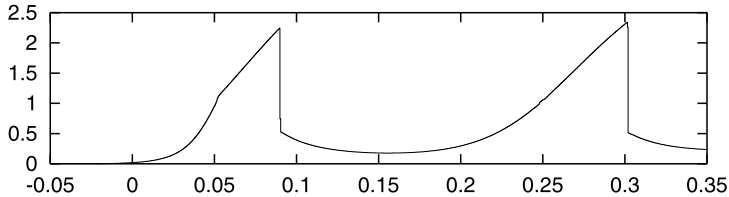

Figure 5. Mach number along the axis, steady three-dimensional axisymmetric finite volume solution with two shocks.

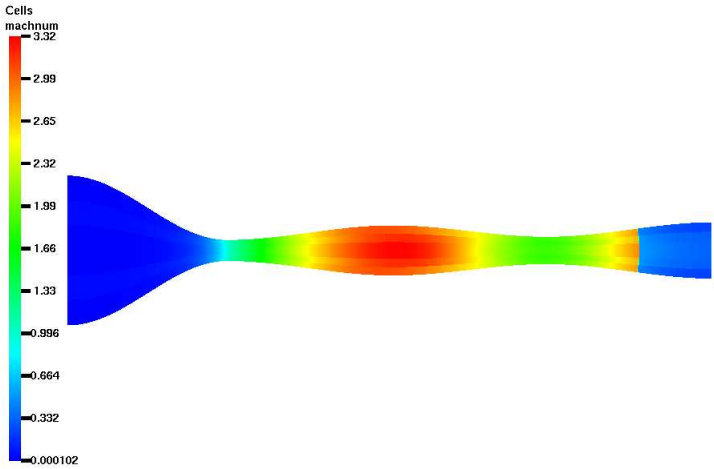

Figure 6. Mach number gray scale map, steady three-dimensional axisymmetric finite volume solution with exactly one shock.

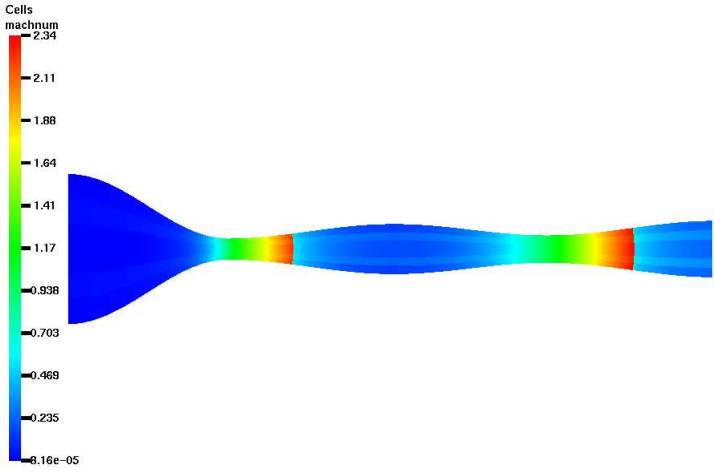

Figure 7. Mach number gray scale map, steady three-dimensional axisymmetric finite volume solution with two shocks.

4.2. A triple nozzle

Let us present an example of a *triple nozzle*, which is not frequently discussed in the literature, maybe due to its limited industrial application. Nevertheless, it is suitable for our purposes as we can construct three different solutions to stationary compressible Euler equations with this geometry.

Let us consider the radius (39) in an interval I given by $x_a = -0.05\,\mathrm{m}$ and $x_b = 0.55\,\mathrm{m}$ as shown in Fig. 8.

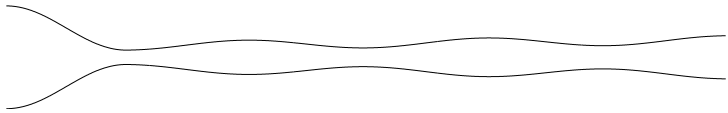

Figure 8. Geometry of the triple nozzle.

In this case, the boundary conditions are chosen as $p_a = 60000\,\mathrm{Pa}$, $\theta_a = 368.16\,\mathrm{K}$ and $p_b = 20000\,\mathrm{Pa}$. The positive value of the inlet velocity u_a is, analogously as in the previous example, computed in such a way that the nozzle works in the Laval regime. The inlet density ϱ_a is computed using (4).

The interval I is divided equidistantly into $N_{\mathrm{elem}} = 1500$ finite volumes. In Figs. 9, 10 and 11, we show three different solutions to Problem 1. Again, analytical solutions are depicted by solid lines and the steady finite volume solutions are represented by dashed lines. In Figs. 12 to 17, results of the corresponding axisymmetric computation are shown. This time, we used a structured triangular grid with 4500 elements.

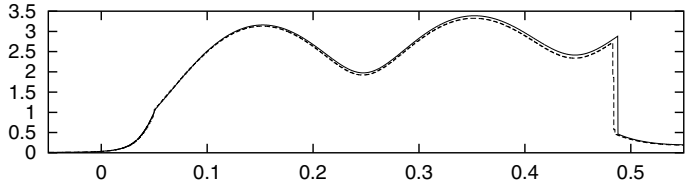

Figure 9. Mach number, quasi-one-dimensional exact (solid line) and steady finite volume (dashed line) solution with exactly one shock.

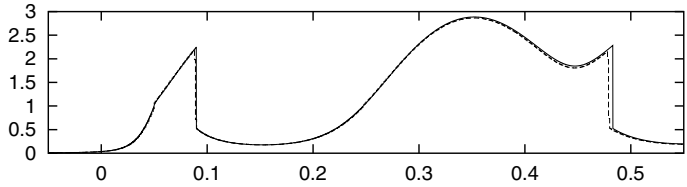

Figure 10. Mach number, quasi-one-dimensional exact (solid line) and steady finite volume (dashed line) solution with exactly two shocks.

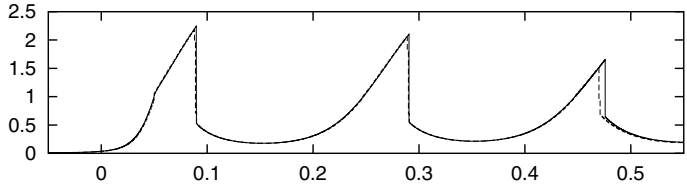

Figure 11. Mach number, quasi-one-dimensional exact (solid line) and steady finite volume (dashed line) solution with three shocks.

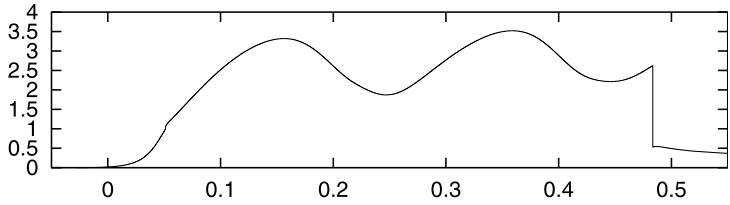

Figure 12. Mach number along the axis, steady three-dimensional axisymmetric finite volume solution with exactly one shock.

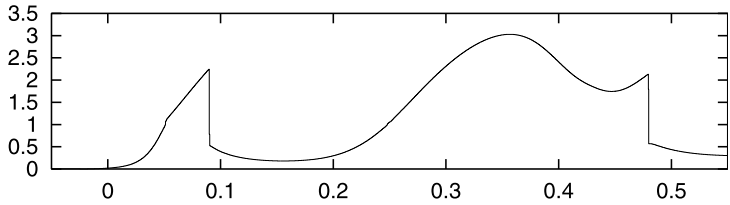

Figure 13. Mach number along the axis, steady three-dimensional axisymmetric finite volume solution with exactly two shocks.

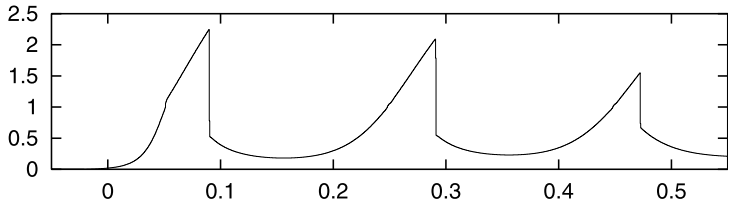

Figure 14. Mach number along the axis, steady three-dimensional axisymmetric finite volume solution with three shocks.

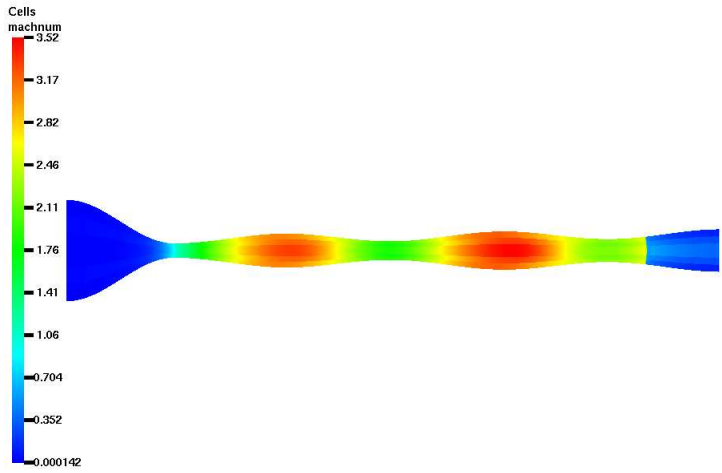

Figure 15. Mach number gray scale map, steady three-dimensional axisymmetric finite volume solution with exactly one shock.

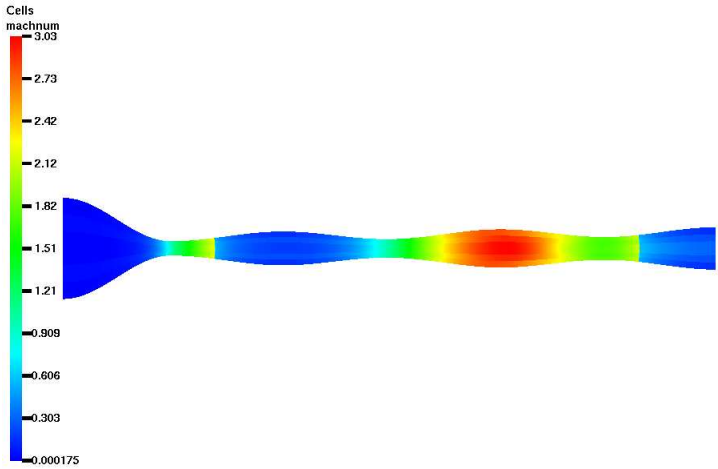

Figure 16. Mach number gray scale map, steady three-dimensional axisymmetric finite volume solution with exactly two shocks.

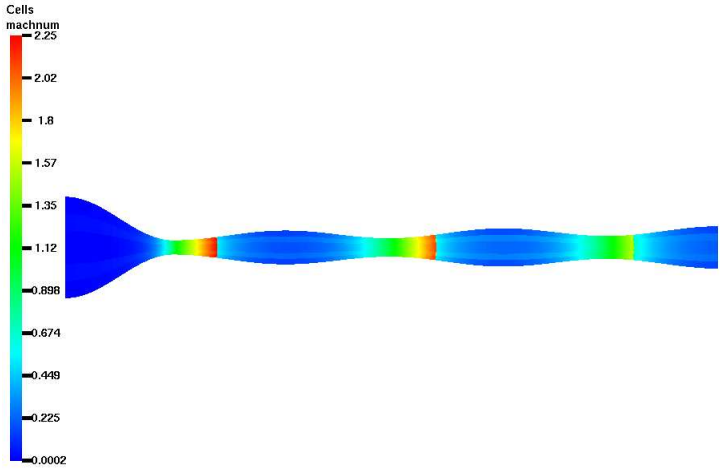

Figure 17. Mach number gray scale map, steady three-dimensional axisymmetric finite volume solution with three shocks.

In both examples, the reader can observe a good agreement between the analytical and numerical results. This means that the reason for non-uniqueness does not lie in the quasi-one-dimensional simplification of the compressible Euler equations. The presented numerical experiments document that non-uniqueness is also present in general three-dimensional equations.

References

[1] *M. Feistauer*: Mathematical Methods in Fluid Dynamics. Longman Scientific & Technical, Harlow, 1993.

[2] *J. Felcman, P. Šolín*: On the construction of the Osher-Solomon scheme for 3D Euler equations. East-West J. Numer. Math. *6* (1998), 43–64.

[3] *C. Hirsch*: Numerical Computation of Internal and External Flows, Vol. 2. J. Wiley & Sons, Chichester, 1990.

[4] *D. D. Knight*: Inviscid Compressible Flow. The Handbook of Fluid Dynamics. CRC, 1998.

[5] *L. D. Landau, E. M. Lifschitz*: Fluid Mechanics. Pergamon Press, London, 1959.

[6] *H. Ockendon, A. B. Tayler*: Inviscid Fluid Flow. Springer-Verlag, New York-Heidelberg-Berlin, 1983.

[7] *H. Ockendon, J. R. Ockendon*: The Fanno Model for Turbulent Compressible Flow. Preprint, OCIAM. Mathematical Institute, Oxford University, Oxford, 2001.

[8] *S. Osher, F. Solomon*: Upwind difference schemes for hyperbolic systems of conservation laws. Math. Comp. *38* (1982), 339–374.

[9] *A. H. Shapiro*: The Dynamics and Thermodynamics of Compressible Fluid Flow, Vol. 1. The Ronald Press Co., New York, 1953.

[10] *J. L. Steger, R. F. Warming*: Flux vector splitting of the inviscid gasdynamics equations with applications to finite-difference methods. J. Comput. Phys. *40* (1981), 263–293.

[11] *A. Terenzi, N. Mancini, F. Podenzani*: Transient Compressible Flow in Pipelines: a Godunov-type Solver for Navier-Stokes Equations. Preprint, 2000.

[12] *E. Truckenbrodt*: Fluidmechanik, Band 2. Springer-Verlag, Berlin-Heidelberg-New York, 1980.

[13] *G. Vijayasundaram*: Transonic flow simulation using upstream centered scheme of Godunov type in finite elements. J. Comput. Phys. *63* (1986), 416–433.

[14] *A. J. Ward-Smith*: Internal Fluid Flow, The Fluid Dynamics of Flow in Pipes and Ducts. Clarendon Press, Oxford, 1980.

[15] *P. Wesseling*: Principles of Computational Fluid Dynamics. Springer-Verlag, Berlin, 2000.

Authors' addresses: *P. Šolín*, CAAM, Rice University, Houston, TX 77251-1892, U.S.A., e-mail: `solin@rice.edu`; *K. Segeth*, Mathematical Institute of the Academy of Sciences of the Czech Republic, Žitná 25, 115 67 Praha 1, Czech Republic, e-mail: `segeth@math.cas.cz`.